Article:
Yu, W., Bau, D. orcid.org/0000-0002-0730-5478, Mayer, A. et al. (2 more authors) (2023) Investigating the impact of seawater intrusion on the operation cost of groundwater supply in island aquifers. Water Resources Research, 59 (10). e2023WR034798. ISSN 0043-1397

https://doi.org/10.1029/2023WR034798

AGU ADVANCING EARTH AND SPACE SCIENCES

Water Resources Research

RESEARCH ARTICLE
10.1029/2023WR034798

Special Section:
Modeling, simulation, and big data techniques in subsurface fluid flow and transport

Investigating the Impact of Seawater Intrusion on the Operation Cost of Groundwater Supply in Island Aquifers

Weijiang Yu[1], Domenico Baù[1], Alex S. Mayer[2], Lauren Mancewicz[3], and Mohammadali Geranmehr[1]

[1]Department of Civil and Structural Engineering, University of Sheffield, Sheffield, UK, [2]Department of Civil Engineering, University of Texas at El Paso, El Paso, TX, USA, [3]Department of Civil, Environmental, and Geospatial Engineering, Michigan Technological University, Houghton, MI, USA

Key Points:

- Effects of pumping patterns (pump depth, rate and well location) on island groundwater supply cost and seawater intrusion (SWI) are studied
- Shallow pumping near the island center is cost-effective but causes more severe SWI, that is, a conflict between economic cost and SWI control
- Controlling SWI by limiting water table drawdown usually leads to selecting more expensive groundwater supply strategies

Correspondence to:
W. Yu,
wyu18@sheffield.ac.uk

Citation:
Yu, W., Baù, D., Mayer, A. S., Mancewicz, L., & Geranmehr, M. (2023). Investigating the impact of seawater intrusion on the operation cost of groundwater supply in island aquifers. *Water Resources Research*, *59*, e2023WR034798. https://doi.org/10.1029/2023WR034798

Received 2 MAR 2023
Accepted 23 SEP 2023

Author Contributions:
Conceptualization: Weijiang Yu
Data curation: Weijiang Yu
Formal analysis: Weijiang Yu, Domenico Baù
Investigation: Weijiang Yu, Domenico Baù, Alex S. Mayer
Methodology: Weijiang Yu
Software: Weijiang Yu
Supervision: Domenico Baù, Alex S. Mayer, Lauren Mancewicz, Mohammadali Geranmehr

Abstract Managing fragile island freshwater resources requires identifying pumping strategies that trade off the financial cost of groundwater supply against controlling the seawater intrusion (SWI) associated with aquifer pumping. In this work, these tradeoffs are investigated through a sensitivity analysis conducted in the context of an optimization formulation of the groundwater management problem, which aims at minimizing the groundwater supply operation cost associated with groundwater pumping and desalination treatment, subject to constraints on SWI control, as quantified by the water table drawdown over the well (Δs), the reduction in freshwater volume (ΔFV) in the aquifer, or the salt mass increase (ΔSM) in the aquifer. This study focuses on a simplified two-dimensional model of the San Salvador Island aquifer (Bahamas). Pumping strategies are characterized by the distance of the pumping system from the shoreline (WL), the abstraction screen depth (D) and overall pumping rate (Q), constituting the decision variables of the optimization problem. We investigate the impacts of pumping strategies on the operation cost, Δs, ΔFV and ΔSM. Findings indicate increasing D or decreasing WL reduces Δs, ΔFV and ΔSM, thus preserving the aquifer hydrogeologic stability, but also leads to extracting saltier groundwater, thus increasing the water treatment requirements, which have a strong impact on the overall groundwater supply cost. From a financial perspective, groundwater abstraction near the island center and at shallow depths seems the most convenient strategy. However, the analysis of the optimization constraints reveals that strategies where the pumping system approaches the island center tend to cause more severe SWI, highlighting the need to trade off groundwater supply cost against SWI control.

1. Introduction

Coastal regions are the most densely populated areas in the globe, with more than half of the world's population residing within 100 km of a shoreline (Kazakis et al., 2018; Tomaszkiewicz et al., 2014). In these regions, intense water demand often forces local communities to rely on groundwater to supplement surface freshwater. Coastal aquifers are normally characterized by a freshwater-seawater contact zone, in which seaward discharging freshwater overlies the landward movement of seawater due to its lighter density (Kishi & Fukuo, 1977). When the abstraction rate exceeds the natural freshwater recharge, the seaward hydraulic gradient drops, causing the landward advancement of saltwater in aquifers, known as SWI. SWI increases the salinity level of groundwater, directly endangering access to subsurface freshwater for coastal communities (Agoubi, 2021; Jasechko et al., 2020). To protect coastal subsurface freshwater from SWI, many solutions have been proposed, including subsurface physical barriers (Abdoulhalik et al., 2017), flow barriers (Botero-Acosta & Donado, 2015; Bray & Yeh, 2008) and surface recharge canals (Motallebian et al., 2019). Among these measures, optimal design and management of groundwater abstraction has gained much attention over the past decades, to address the conflict between groundwater abstraction and SWI control.

Simulation-optimization (SO) frameworks have been proven to be effective tools to identify optimal groundwater management strategies (Baù & Mayer, 2006; Christelis & Mantoglou, 2019; Dey & Prakash, 2020; Mayer et al., 2002; Rajabi & Ketabchi, 2017; D. K. Roy & Datta, 2020). A SO framework is typically characterized by three components: an optimization formulation to the groundwater management problem, a process-based groundwater simulation model and an optimization algorithm. The optimization formulation requires defining the management goals as objective functions and constraints, as well as the decision variables (DVs) that identify the management policies, that is, groundwater pumping schemes. Once DVs are selected, the simulation model is used to estimate the state variables (SVs), which define the aquifer response to pumping. DVs and SVs are then

Validation: Weijiang Yu, Domenico Baù, Alex S. Mayer, Lauren Mancewicz, Mohammadali Geranmehr
Visualization: Weijiang Yu
Writing – original draft: Weijiang Yu
Writing – review & editing: Weijiang Yu, Domenico Baù

used to calculate objective functions and verify compliance with constraints. The optimization algorithm is the mathematical tool that conducts the search for the optimal set of DVs.

Coastal groundwater management has been most often formulated as a single-objective problem, aiming to maximize the total pumping rate from production wells subject to constraint conditions (Coulon et al., 2022; Dey & Prakash, 2020; Karatzas & Dokou, 2015; Kopsiaftis et al., 2019; Rajabi & Ketabchi, 2017; Sedki & Ouazar, 2011). Several authors have considered objective functions that relate to either the cost of or the economic revenue of groundwater supply. In Yin et al. (2020), the objective function consisted of the energy cost for groundwater pumping. Mayer et al. (2002) proposed an objective function that included capital and operation costs associated with both pumping and treatment, whereas El-Ghandour and Elbeltagi (2020) considered the objective of maximizing the revenue from groundwater supply, which accounted also for pumping costs. In Qahman et al. (2005), the objective function consisted of the benefit from groundwater supply minus the desalination cost, which accounts for potential pumping schemes that produce brackish or salt water.

When considering management goals that represent either revenue or cost, objectives result typically in complex, irregular, and potentially discontinuous functions of DVs and SVs (Mayer et al., 2002; Yin et al., 2020). Since these may pose significant challenges to identifying optimal solutions, several authors have adopted measures to simplify the objective functions. For example, Javadi et al. (2012) and Ketabchi and Ataie-Ashtiani (2015) calculated pumping costs based on extraction rates and total dynamic heads, whereas Qahman et al. (2005) formulated treatment costs as proportional to the product of abstracted volumes and desalination coefficients. Likewise, El-Ghandour and Elbeltagi (2020), Park and Shi (2015), and Yang et al. (2021) evaluated the monetary benefits of groundwater usage as linearly proportional to the pumping intensity.

In general, management constraints can be subdivided into three main groups. The first group includes limitations on ranges of the variability of DVs, such as pumping rates, well locations and screen depths (Javadi et al., 2015), and total groundwater demand (Fan et al., 2020; Kourakos & Mantoglou, 2011). A second group considers restrictions to SWI due to aquifer pumping, typically formulated in relation to groundwater salinity. Groundwater salinity constraints have been expressed in terms of freshwater-saltwater interface location when neglecting solute dispersion effects, as at regional aquifer scales, which have allowed to adopt "sharp-interface" models (Christelis & Mantoglou, 2016; Dey & Prakash, 2020; Ferreira da Silva & Haie, 2007; Kopsiaftis et al., 2019; Stratis et al., 2017). At smaller aquifer scales, where the assumption of miscible freshwater and saltwater is needed, salinity constraints have been prescribed as salt concentration limits at control points, such as pumping wells or monitoring wells, which have required the use of variable density flow models that are more complex and computationally more expensive than sharp-interface models (Christelis & Mantoglou, 2019). SWI constraints have also been applied indirectly on hydraulic head, by limiting, for example, seaward hydraulic gradients or the water table drawdown at given monitoring points (Karatzas & Dokou, 2015; Pramada et al., 2018; Yang et al., 2018). A third group of SWI constraints involves the economic aspects of management. For example, Ranjbar and Mahjouri (2019) addressed groundwater management problems, in which water administrators set an expected benefit for groundwater supply by capping maximum pumping costs.

Some scholars have addressed the tradeoffs between achieving competing management objectives and complying with constraints by using multiple-objective optimization approaches, in which constraints are transformed into additional objective functions (El-Ghandour & Elbeltagi, 2020; Fan et al., 2020; Park & Shi, 2015). Compared with the single-objective management problem, these approaches have the advantage of providing optimal management strategies under varied constraint scenarios.

In the management of groundwater in coastal aquifers that are vulnerable to SWI, the cost of groundwater supply appears to be a strong indicator of optimality as it depends significantly on the cost of desalination (Javadi et al., 2015; McKinney & Lin, 1994), which implicitly tends to exclude pumping strategies that can cause SWI. It appears, however, that the minimization of the SWI extent should be considered as an explicit objective for stability and sustainability of water resources. In this respect, Song et al. (2018) adopted, as a main objective, the minimization of total salt mass increase in the aquifer. Triki et al. (2017) and Zekri et al. (2015) used the minimization of the mean drawdown near the shoreline, and Fan et al. (2020) and Rajabi and Ketabchi (2017) targeted the minimization of concentrations at monitoring wells. T. Roy et al. (2016) adopted a two-objective optimization problem to manage utilization of coastal groundwater, which maximized farmer benefit, while minimizing SWI through a sustainability index function expressed by the water table elevation and salinity at specific monitoring

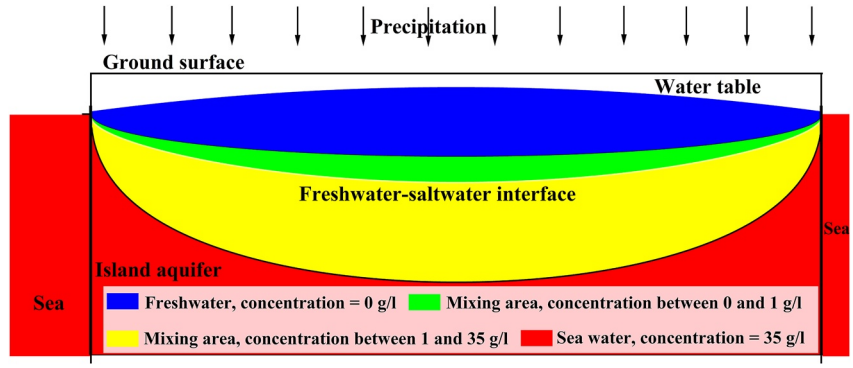

Figure 1. Cross-section diagram of a freshwater lens in an island aquifer. The thickness of the lens depends mainly on the aquifer hydraulic conductivity and the intensity of water infiltration from precipitation.

locations. While this approach enables preventing local salinization, for example, at pumping wells, it may not ensure SWI alleviation on the whole aquifer.

To date, most SO applications to SWI management have considered "classic" coastal aquifers, which are typically included in larger and elongated geological formations stretching along the coastline of continents, and only a few studies have focused specifically on island aquifers (Coulon et al., 2022; Kourakos & Mantoglou, 2015), which are characterized by very particular hydrogeological settings. In this type of aquifer, fresh groundwater resources are generally lens-shaped and sustained solely by groundwater recharge from local precipitation (Figure 1). The freshwater thickness is often of the order of a few meters (Fetter, 1972), which makes these aquifers extremely vulnerable to SWI. Excessive groundwater abstraction may thus lead to depletion of freshwater resources, aquifer salinization, and increased costs for water desalination. In these situations, curtailed pumping may ultimately result as the only viable option for maintaining or re-establishing lens aquifers.

In this study, we approach the management of groundwater in island aquifers as a single-objective optimization problem, with the primary objective being the minimization of operating costs associated with groundwater extraction and desalination treatment. Our focus is specifically on addressing the cost increase resulting from rising groundwater demand, which is directly influenced by population density. While SWI has a direct impact on management costs due to its effect on desalination intensity, we also establish explicit constraints to control SWI.

To assess the interplay between management costs and these constraints, we adopt a SO analysis approach, considering a cost objective function and three types of SWI constraints, both individually and in combination. It is important to note that we do not adopt any specific optimization algorithm to solve the formulated management problems. Instead, we design a large set of potential groundwater abstraction strategies, and by modeling the aquifer's responses to these strategies, we can identify the optimal pumping scheme and its associated management cost through full enumeration evaluation (e.g., Beheshti et al., 2022) within such a set when SWI control constraints are specified. Finally, by varying the variable bounds of these constraints, we can then identify various corresponding optimal pumping strategies.

This enables us to conduct, within an optimization context, a sensitivity analysis of the optimal groundwater supply costs while aiming to minimize SWI, providing insights into sustainable island groundwater use. Such a sensitivity analysis is conducted on a simplified two-dimensional aquifer, based on hydrogeological conditions observed in the island aquifer of San Salvador Island, Bahamas. The management cost takes into of the expenses associated with groundwater pumping and the desalination process required to ensure the salt concentration in water meets potability standards.

This paper is organized as follows. The next section presents the simulation model for SWI, the optimization formulation of the management problem, that is, the objective function and its constraints, and the sensitivity scenarios considered for the SWI control indicators. Simulation results and their discussion are provided in the following section. The last section presents the conclusions drawn from the investigation.

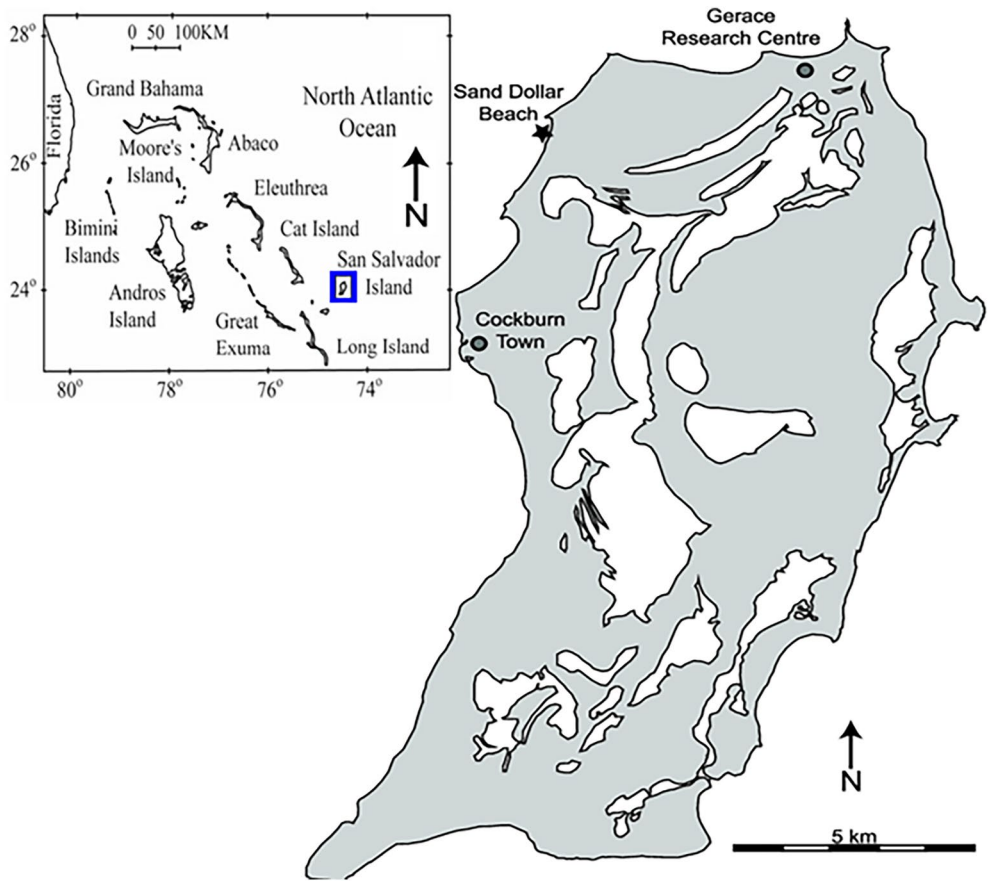

Figure 2. Location map of San Salvador Island (Moore, 2009). The dark gray and the light gray areas represent land and surface water, respectively.

2. Methodology

The goal of this study is to investigate the effects of groundwater pumping strategies on operation cost and SWI, using the San Salvador Island aquifer as a case study. San Salvador Island is located within the Bahamian Archipelago (Figure 2), about 600 km east-southeast of Miami, and sits on a small, isolated carbonate platform (Ho et al., 2014; McGee et al., 2010). The island is about 20 km long north-to-south and has an average width west-to-east of approximately 8 km (Martin & Moore, 2008). The topography is dominated by consolidated carbonate dune ridges, with elevations between 10 and 20 m above sea level (Davis & Johnson, 1989). Characterized by a subtropical climate, San Salvador Island has an annual temperature ranging between 22 and 28°C (McGee et al., 2010) and annual precipitation and potential evaporation of 1,000–1,250 mm/year and 1,250–1,375 mm/year, respectively (Moore, 2009).

2.1. Numerical Simulation of SWI in the San Salvador Island Aquifer

This work applies the SEAWAT model to simulate the SWI process in the island aquifer. SEAWAT couples the groundwater flow model MODFLOW and the solute transport model MT3DMS to solve the variable-density flow equations using a finite-difference numerical approach (Kourakos & Mantoglou, 2013; Langevin et al., 2007; Yao et al., 2019). Since the SEAWAT groundwater model can account for water density variations that depend on salt concentration, it is well-suited for simulating flow in aquifers characterized by freshwater-seawater interactions.

In the investigation of the island groundwater abstraction management, a simplified two-dimensional "cross-section" model is adopted. The island cross-section model is constructed as a rectangular domain, with a length of 8,000 m, a height of 480 m, and a width of 1 m. The aquifer domain is discretized into a finite-difference regular grid with cells of size $8 \times 8 \times 1$ m. Two additional grid columns are used to represent the boundary

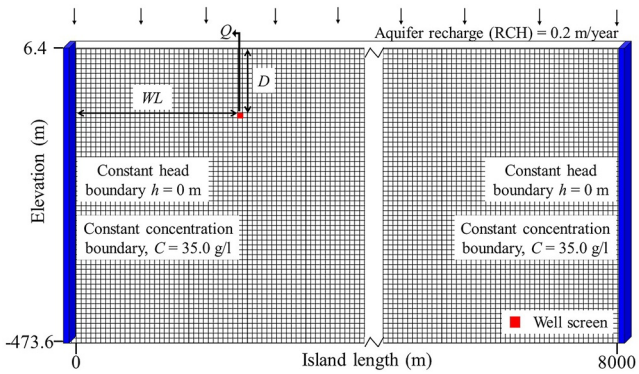

Figure 3. Island aquifer SEAWAT cross-sectional model grid along with the associated boundary conditions. The pumping system is simulated as a single cell located at depth *D* from the ground surface and distance WL from the shoreline.

conditions at the leftmost and rightmost ends of the domain, so that the finite-difference grid is made up by 1,002 columns and 60 rows, for a total of 60,120 cells. The pumping system is represented by a point sink located at a depth *D*, a distance WL from the shoreline, and a pumping rate *Q*, which represents the volume of groundwater extracted per unit time and per unit aquifer width.

Figure 3 shows a conceptualization of the aquifer domain along with the numerical model grid and its boundary conditions. A no-flow boundary is prescribed at the model bottom. The model top is a specified-flux boundary, reflecting the aquifer recharge from precipitation, which is assumed to be 0.2 m per year (Gulley et al., 2016). At the left and right boundaries, a constant head of 0.0 m is prescribed over the water column, which represents the sea level (at the datum). At the same boundaries, a constant concentration of 35.0 g/L is imposed, which represents the salt content in seawater.

To model SWI effects from groundwater abstraction at steady-state, the flow and solute transport are simulated as transient state processes with a sufficiently large period of constant groundwater pumping. A "baseline" scenario is first developed to simulate the island freshwater lens under steady-state conditions of natural groundwater recharge from precipitation only. This serves as the initial condition to model the aquifer freshwater distribution under various scenarios of groundwater pumping. For the simulations involving groundwater pumping, SEAWAT is run until steady-state is reached, which is typically between 2 and 30 years depending on the simulated pumping scheme. Correspondingly, the required CPU time for each simulation varies from a minimum of about 15 min to a maximum of over 1 hr Table 1 provides a list of the relevant parameters adopted in the simulation model introduced above. These parameters are drawn from published works (Gulley et al., 2016; Holding & Allen, 2015) that have used San Salvador Island or nearby island aquifers as test cases.

2.2. Groundwater Management Formulation

The primary objective of the island groundwater management is to identify cost-optimal pumping strategies for prescribed groundwater demand levels. Pumping strategies are characterized by three DVs, the depth *D* [L]

Table 1
Model Parameters Used for Seawater Intrusion Simulation in the San Salvador Island Aquifer

Model component	Parameters	Units	Values
Groundwater Flow	Aquifer recharge (RCH)	m/year	0.2
	Effective porosity	\	0.15
	Specific elastic storage	m^{-1}	1.0×10^{-5}
	Specific yield	\	0.15
	Horizontal hydraulic conductivity (HK)	m/day	50.0
	HK transversal anisotropy ratio	\	1.0
	HK vertical anisotropy ratio	\	1.0
Solute Transport	Longitudinal dispersivity	m	1.0
	Transversal dispersivity	m	0.1
	Vertical dispersivity	m	0.01
	Molecular diffusion coefficient	m^2/s	1.0×10^{-9}
	Aquifer recharge concentration	g/L	0
Density dependence	Freshwater density	kg/m^3	1,000
	Seawater density	kg/m^3	1,025
	Density/concentration slope[a]	\	0.7143

[a]The water density ρ_w [kg/m^3] varies linearly with the salt concentration C [kg/m^3] through the equation $\rho_w = 1{,}000 + 0.7143 \cdot C$.

at which pumping occurs, the distance WL [L] of the pumping system from the shoreline, and the intensity of constant pumping Q [L^2T^{-1}]. The management cost f_{OC} accounts for two main components: the pumping operation cost f_p, and the treatment operation cost f_t, per unit aquifer width and unit time [$\$L^{-1}T^{-1}$]. The former is the cost of energy utilization for lifting groundwater to the ground surface, whereas the latter is the cost of desalination by reverse osmosis (RO), which is required when the salt concentration in water exceeds 1.0 g/L, in accordance with World Health Organization guidelines for drinking water (Yao et al., 2019).

The cost objective function is formulated as:

$$f_{OC} = f_p(Q, h, C) + f_t(Q, C) \tag{1}$$

where h [L] and C [ML^{-3}] are state variables, which represent the hydraulic head at the well screen and the salt concentration in the extracted water, respectively. Both h and C are functions of the DVs (D, WL, Q). f_p is expressed as (Mayer et al., 2002):

$$f_p(Q, h, C) = \rho_w(C) \cdot g \cdot \left(z_{gs} - h\right) \cdot Q \cdot c_e \tag{2}$$

where ρ_w is the water density, which depends on the salt concentration C (Table 1), g denotes gravitational acceleration [LT^{-2}], and z_{gs} represents the ground surface elevation [L], set equal to 15.0 m. The coefficient c_e represents the unit energy cost [$\$M^{-1}L^{-2}T^2$], assumed equal to 0.1848 \$/kWh. The treatment cost, f_t, is estimated as (Avlonitis et al., 2012):

$$f_t(Q, C) = \rho_w(C) \cdot \mathrm{SEC}(C) \cdot Q \cdot c_e \tag{3}$$

where SEC [L^2T^{-2}] is the specific (per unit mass) energy consumption for water desalination (Stillwell & Webber, 2016), which depends on the salt concentration C. A detailed description of SEC is presented in Appendix A.

The formulation of the island groundwater management problem is completed by two groups of constraints. The first group sets the range of variability of the DVs (D, WL, Q). The pumping depth D is subject to the inequality:

$$D_{min} \le D \le D_{max} \tag{4}$$

where D_{min} and D_{max} are the absolute depths below the groundwater surface, equal to 12.6 and 484.6 m, respectively.

Since the model grid (Figure 3) is symmetric with respect to island central axis, the distance WL cannot exceed half of the island length L = 8,000 m. WL is thus constrained as:

$$WL_{min} \le WL \le WL_{max} \tag{5}$$

with WL_{min} equal to $0.05 \cdot L$ and WL_{max} equal to $0.5 \cdot L$. The pumping rate Q depends on the groundwater demand, which may be estimated based on the population density and the per capita water consumption and needs to be constrained in relation to the aquifer recharge rate RCH. Here, Q is assumed to be subject to:

$$Q_{min} \le Q \le Q_{max} \tag{6}$$

with Q_{min} equal to $0.05 \cdot RCH \cdot L$ and Q_{max} equal to $0.2 \cdot \mathrm{RCH} \cdot L$. These values have been selected to cover a range of variability for Q large enough to study its effects on SWI and groundwater supply cost.

A second group of constraints is considered to minimize the extent of the SWI, thus addressing the environmental sustainability of groundwater abstraction. SWI is quantified by three indicators: the hydraulic head drawdown scaled to the water table elevation over the pumping system, the reduction in aquifer freshwater volume, and the increase in aquifer salt mass.

The drawdown at the pumping well is subject to the constraint:

$$\Delta s \le \Delta s_{max} \tag{7}$$

Table 2
Decision Variable Values Considered for the Candidate Pumping Strategies Selected for Island Aquifer Management

Decision variable	Discrete values[a]													
D (m)	12.6	28.6	44.6	60.6	76.6	84.6	92.6	100.6	108.6	124.6	132.6	164.6	244.6	484.6
WL (m)	$0.125 \cdot L$					$0.25 \cdot L$				$0.375 \cdot L$			$0.5 \cdot L$	
Q (m^2/d)	$0.05 \cdot RCH \cdot L$					$0.1 \cdot RCH \cdot L$				$0.15 \cdot RCH \cdot L$			$0.2 \cdot RCH \cdot L$	

[a]L = 8,000 m and RCH = 0.2 m/year are the hypothesized aquifer length and recharge rate, respectively.

where Δs is calculated as the percentage of water table drawdown at the well location with respect to the original water table level, and Δs_{max} is the maximum allowed value for Δs, which is calculated as:

$$\Delta s = \frac{H_0(WL) - H(D, WL, Q)}{H_0(WL)} \cdot 100 \leq \Delta s_{\max}\,[\%] \tag{8}$$

where $H_0(WL)$ is the water table level over the pumping system prior to pumping (baseline scenario), and $H(D, WL, Q)$ is the corresponding steady-state water table level during pumping, which depends on the DV set.

The reduction in aquifer freshwater volume is constrained as:

$$\Delta FV \leq \Delta FV_{\max} \tag{9}$$

where $\Delta FV(D, WL, Q)$ is the percentage of the groundwater freshwater volume decrease in the aquifer:

$$\Delta FV = \frac{FV_0 - FV(D, WL, Q)}{FV_0} \cdot 100 \leq \Delta FV_{\max}\,[\%] \tag{10}$$

where FV_0 is the freshwater volume prior to pumping (baseline scenario), and FV is the corresponding steady-state volume during pumping. ΔFV_{max} is the maximum allowed value for ΔFV. FV is calculated by spatial integration of the pore volume in those grid cells where the simulated salt concentration is less than 1 g/L.

The aquifer salt mass increase is subject to the inequality:

$$\Delta SM \leq \Delta SM_{\max} \tag{11}$$

where ΔSM is the percentage of salt mass increase in the aquifer, given by:

$$\Delta SM = \frac{SM(D, WL, Q) - SM_0}{SM_0} \cdot 100 \leq \Delta SM_{\max}\,[\%] \tag{12}$$

where SM_0 is the total salt mass in the aquifer prior to pumping and SM is the total salt mass at steady state during pumping. ΔSM_{max} is the maximum allowed value for ΔSM. SM values are calculated by integrating the salt concentration multiplied by the pore volume over all model grid cells.

2.3. Optimization Scenarios

It is worth noting that, for any given DV set (D, WL, Q), the calculations of the objective function (Equations 1–3) and the management constraints (inequalities 7, 9, and 11) require the values of the SVs, h and C, and corresponding SWI metrics Δs, ΔFV, and ΔSM, which are here calculated using the SEAWAT model. Rather than relying on the solution of the optimization problem through the application of a particular optimization algorithm, our investigation is based on the analysis of a pre-fixed large set of groundwater abstraction strategies (i.e., SEAWAT model runs), expressed as a prescribed ensemble of DV sets, and the comparison of their "performance" in terms of management cost (Equation 1) and constraints (inequalities 7, 9, and 11). The use of a discrete set of abstraction strategies enables the analysis of the impact of both separate and combined SWI constraints, as well as the prescribed SWI bounds, on the pumping strategies that lead to the minimum management cost, and the magnitude of the cost itself.

Table 2 provides a description of the ensemble of DV sets (D, WL, Q) used in this study. The pumping system depth D varies over 14 discrete values, which meet inequality (4) and are mainly concentrated in the shallower

Table 3
Threshold Values Used in the Sensitivity Analysis of Potential Seawater Intrusion Constraints on the Optimal Management Cost

Upper bound	Values (%)					
Δs_{max}	5	10	15	20	25	30
ΔFV_{max}	5	10	15	20	25	30
ΔSM_{max}	0.5	1	2	3	4	5

portion of the lens aquifer, where most freshwater is found prior to pumping. As for *WL*, which needs to meet inequality (5), the pumping system may be positioned at 4 alternative regularly spaced locations, from the vicinity of the seashore ($0.125 \cdot L$) to the center of the island ($0.5 \cdot L$). The pumping rate Q is assumed to satisfy four groundwater demand levels, from a minimum of $0.05 \cdot \text{RCH} \cdot L$, to a maximum of $0.2 \cdot \text{RCH} \cdot L$. The combination of these DV values leads to an ensemble of $14 \times 4 \times 4 = 224$ alternative groundwater abstraction strategies, and thus as many SEAWAT model runs. An additional model run is also needed to simulate the baseline "no-pumping" scenario.

Table 3 describes constraint bound values assigned to evaluate the tradeoff between SWI restrictions and the management cost of groundwater abstraction. Both Δs_{max} and ΔFV_{max} (inequalities 7 and 9) are assumed to vary from a stricter lower limit of 5%, to a more relaxed upper limit of 30%, at 5% increments. ΔSM_{max} (inequality 11) is assumed to increase from a minimum of 0.5%, up to a maximum of 5%, representing progressively larger SWI intensities.

In an initial series of tests, cost-optimal pumping strategies are identified among the alternatives presented in Table 2 as if the sole SWI constraint under consideration was represented by either of the inequalities (7), (9) or (11). These tests are designed to provide insight into the impact on the minimum-cost pumping scheme of (a) each individual SWI constraint type and (b) the selected upper bound for that constraint (Table 3).

Next, cost-optimal pumping strategies are investigated by assuming two concurrent SWI constraints. These combined constraint scenarios are presented in Table 4, which shows as many as 12 optimization setups, denoted as Scenarios 1 through 12. The first four scenarios assume SWI constraints imposed on Δs and ΔFV, the second four scenarios consider constraints on Δs and ΔSM, and the remaining scenarios hypothesize constraints on ΔFV and ΔSM. These tests allow for investigating the interplay between SWI constraints and their joint impact on groundwater lens management. Lastly, optimal pumping strategies are investigated by imposing the SWI constraints (7), (9) or (11) jointly, under various upper bound sets, with as many as 8 optimization setups investigated. These scenarios are denoted as Scenario 13 through 20 (see Table 5).

Table 4
Sensitivity Scenarios for Two-SWI-Constraint Combinations

Scenario	Δs_{max}	ΔFV_{max}	ΔSM_{max}
1	10%	10%	–[a]
2	10%	30%	–
3	30%	10%	–
4	30%	30%	–
5	10%	–	1%
6	10%	–	5%
7	30%	–	1%
8	30%	–	5%
9	–	10%	1%
10	–	10%	5%
11	–	30%	1%
12	–	30%	5%

[a]The symbol "–" indicates a constraint condition not in use.

3. Results and Discussion

3.1. Impact of the DVs on Pumping and Desalination Costs

The distribution of groundwater concentration in the baseline scenario, prior to pumping, is depicted in Figure 4. It can be observed that the freshwater lens depth varies from zero in proximity of the shoreline, to about 110 m at the center of the island. Correspondingly, the depth at which seawater is found varies from about 40 m to approximately 165 m.

Figure 5 presents the results of an analysis of the impact of the DVs on the management cost function (Equations 1–3). The data points used for the plots in Figure 5 correspond to the 224 DV combinations (D, WL, Q) presented in Table 2. Figure 5a shows profiles of the hydraulic head h at the well screen with respect to the pumping depth D, the distance to the shoreline *WL*, and the abstraction rate Q. These profiles reveal that: (a) for any given combination of *WL* and Q, with increasing D, h tends to first slightly increase, then drops dramatically at depths around 60 m, and becomes practically constant beyond at depths below 150 m from the ground surface; (b) h tends to increase by increasing *WL*, that is, by moving the well toward the center of the island; (c) h tends to decrease by increasing Q, that is, the hydraulic head at the well screen is lower if the pumping rate higher.

Table 5
Sensitivity Scenarios for Three-SWI-Constraint Combinations

Scenario	Δs_{max} (%)	ΔFV_{max} (%)	ΔSM_{max} (%)
13	10	10	1
14	10	10	5
15	10	30	1
16	10	30	5
17	30	10	1
18	30	10	5
19	30	30	1
20	30	30	5

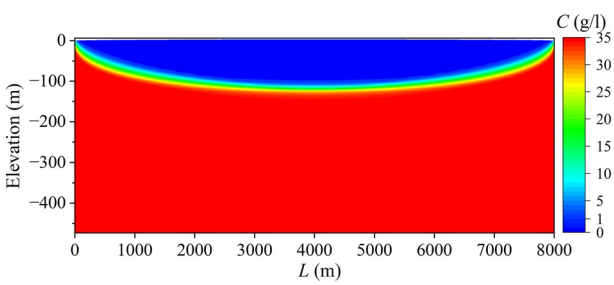

Figure 4. Distribution of groundwater concentration in the baseline scenario.

Figure 5b shows profiles of the salt concentration C of the pumped water with respect to the DVs D, WL, and Q. These profiles reveal that: (a) for D values down to 50 m, C does not exceed 5 g/L, but then increases dramatically reaching the seawater concentration of 35 g/L for D exceeding ~150 m. This is due to the groundwater abstraction being progressively shifted across the freshwater-saltwater transition zone. While the location of this transition zone depends specifically on the thickness of the freshwater lens and the hypothesized mixing conditions, qualitatively similar profiles should be expected for island aquifer settings other than those assumed here; (b) C is seen to increase by decreasing WL, that is, by pumping closer to the shoreline, where the freshwater lens is thinner and higher salinity is found at shallower depth; (c) C increases by increasing Q, that is, the more water is pumped, the higher the salinity, due to the upward movement of salt-rich groundwater below the pumping point (Jakovovic et al., 2011).

Figures 5c and 5d show the profiles of the pumping cost f_p and the desalination cost f_t, respectively, against the pumping depth D, and for different values of the distance WL and the abstraction rate Q. Figure 5c indicates that f_p increases quite slightly if D increases and becomes practically constant for depths exceeding ~150 m. The cost f_p is generally larger if the pumping rate Q is increased and does not seem sensitive to variations of WL. This is an apparent effect due to the logarithmic scale adopted in Figure 5c. A closer look (see Appendix B) reveals that f_p actually decreases if WL increases, that is, if the pumping system is moved closer to the island center. These trends are explained by observing the behavior of h in the DV space (D, WL, Q), as shown in Figure 5a, and noting the dependency of f_p on h and Q in Equation 2.

Figure 5d shows that f_t increases with D and reaches horizontal asymptotes that depend mainly on the pumping rate Q. For any given combination of WL and Q, the treatment cost f_t is relatively low if the pumping system is shallower, that is, for lower D, but increases dramatically for larger D, due to the increase in concentration C, as observed in Figure 5b. However, f_t values become constant at depth larger than 150 m, as C is limited by the seawater concentration of 35 g/L (Figure 4b). The maximum values of treatment cost are observed to be practically proportional to Q, and are generally larger if the pumping system is closer to the shoreline, that is, for lower WL values, due to the reduced thickness of the freshwater lens aquifer (Figure 1).

A comparison of the profiles in Figures 5c and 5d reveals that the treatment cost f_t largely exceeds the pumping cost f_p under most circumstances. In certain pumping conditions, f_t may be up to one order of magnitude larger than f_p. On the other hand, the two cost components are comparable only for lower abstraction rates Q, and for shallow pumping systems (i.e., lower D values) situated toward the center of the island (i.e., larger WL values). These differences are a direct consequence of the remarkably different specific energy consumptions associated with groundwater pumping and desalination.

3.2. Impact of the DVs on Operation Costs and SWI Indicators

Figure 6a shows that, for larger WL and lower Q, f_{OC} tends to decrease with the pumping depth D until this remains within 50–100 m. This happens because groundwater abstraction occurs within the original freshwater lens, so that little or no desalination is required, and the predominant cost component is f_p (Figure 5c). Instead, for lower WL and larger Q, f_{OC} increases along the depth D, since the dominant cost component becomes f_t (Figure 5d). In general, for D larger than 50–100 m, the total cost f_{OC} increases sharply due to the abstraction of groundwater with salt concentration that exceeds the treatment threshold (Figure 5b). The profiles in Figure 6a indicate that, for lower WL and larger Q, the cost-optimal pumping strategies are those with the smallest D. For larger WL and lower Q, however, the cost-optimal pumping strategies are found for intermediate values of D, between 50 and 100 m.

Figures 6b–6d show that the drawdown percentage Δs, the percentage of the freshwater volume decrease ΔFV, and the percentage of salt mass increase

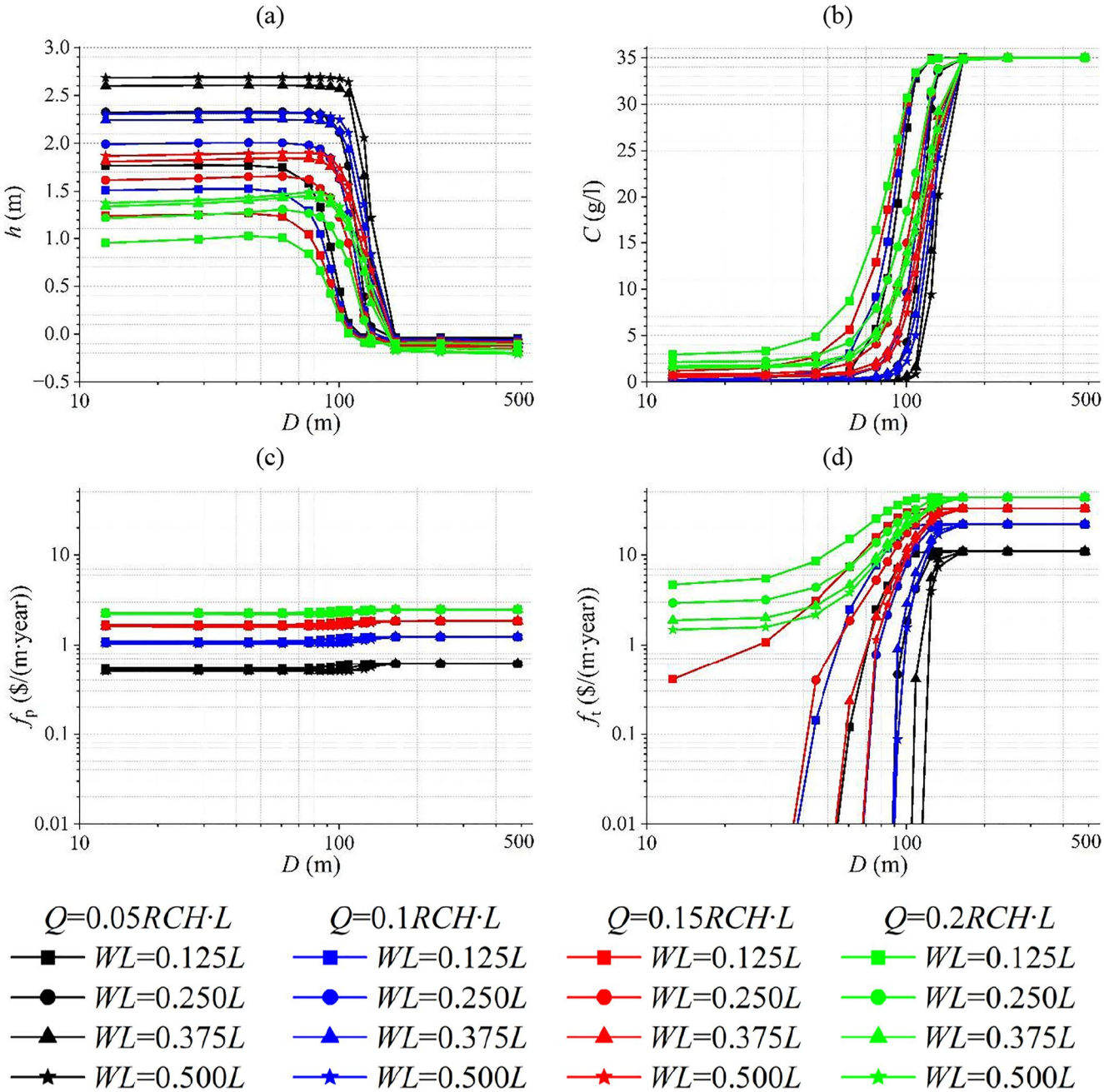

Figure 5. (a) Steady-state water table elevation over the well, h; (b) extracted groundwater salt concentration, C; (c) pump cost f_p and (d) treatment cost f_t for the proposed 224 alternative groundwater abstraction strategies (Table 2). f_t profiles in subpanel (d) falling below 0.01 \$/(m · year) indicate that no desalination is required (i.e., treatment cost is zero).

ΔSM share a similar behavior, generally decreasing with D and increasing with both WL and Q. In Figure 6b, it is interesting to observe that if D is generally over ~150 m, the drawdown is marginally affected by groundwater abstraction and most of the pumped groundwater is resident seawater. In Figures 6c and 6d, the dependency of ΔFV and ΔSM on Q may be explained through simple considerations of aquifer mass balance. At steady state, the abstraction rate Q is provided in part by the freshwater recharge, and in part by the seawater inflow from the shoreline boundaries, with an overall decrease in the freshwater lens volume. If the pumping depth D is increased or the distance WL is decreased, both ΔFV and ΔSM become progressively less significant, and if D is larger than ~150 m, they become negative, which implies an overall increase of the freshwater lens volume as pumping removes salt water from underneath, thus promoting the downward flow of freshwater from recharge.

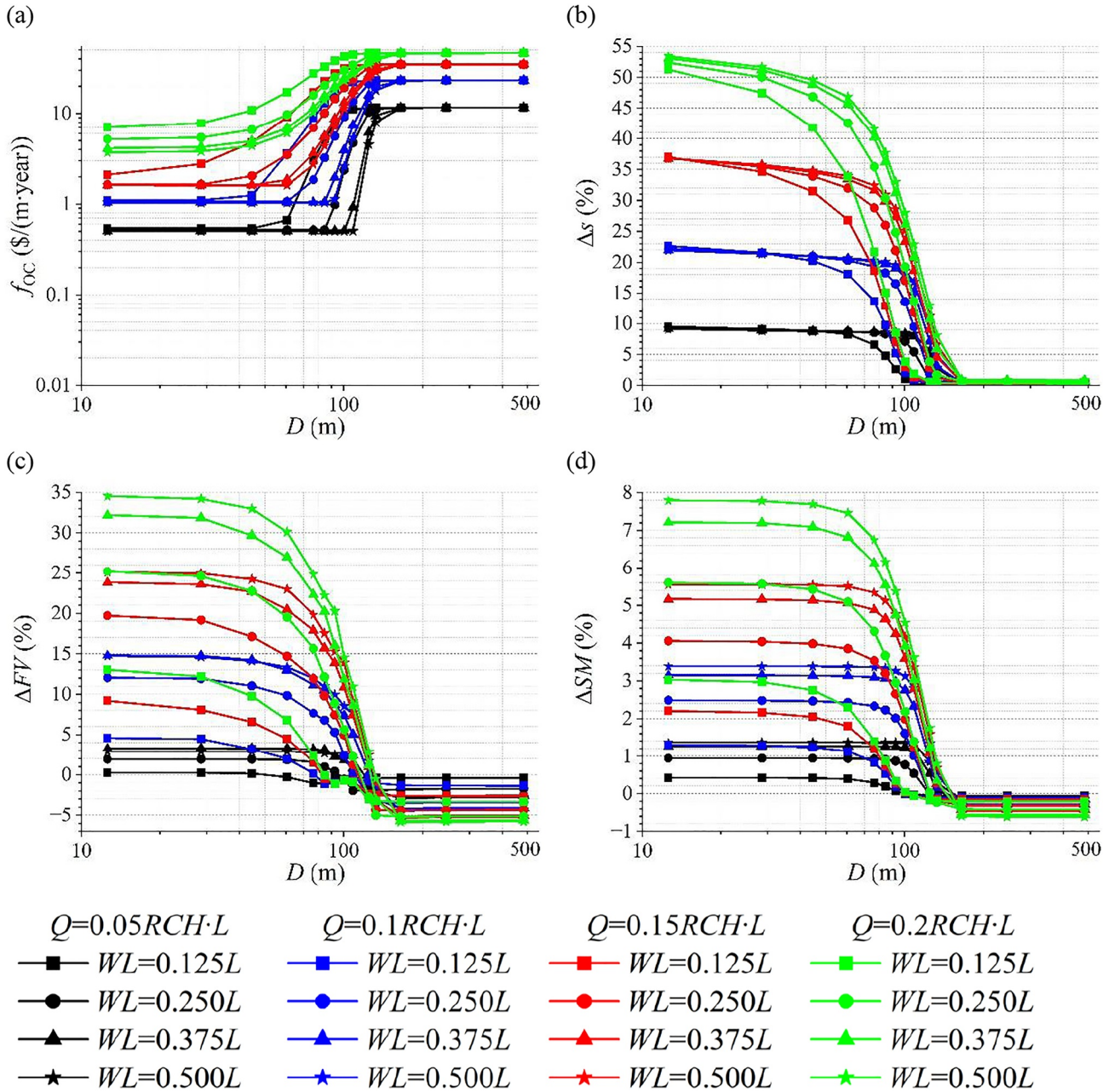

Figure 6. Profiles showing (a) the operation cost f_{OC} and the seawater intrusion indicators (b) Δs, (c) ΔFV and (d) ΔSM for 224 alternative pumping strategies. Legends for the profiles are presented at the figure bottom.

Altogether, the operating cost function f_{OC} and the SWI indicators presented in Figure 6 illustrate the inherent conflicts between the economic cost of groundwater supply and the management SWI. On one hand, for any given demand Q, f_{OC} is minimized by selecting a shallow pumping system situated toward the center of the island center. On another, to limit SWI indicators, such as Δs, ΔFV and ΔSM, it is necessary to select deeper pumping systems and closer to the shoreline, which may massively increase the operation cost due to desalination requirements.

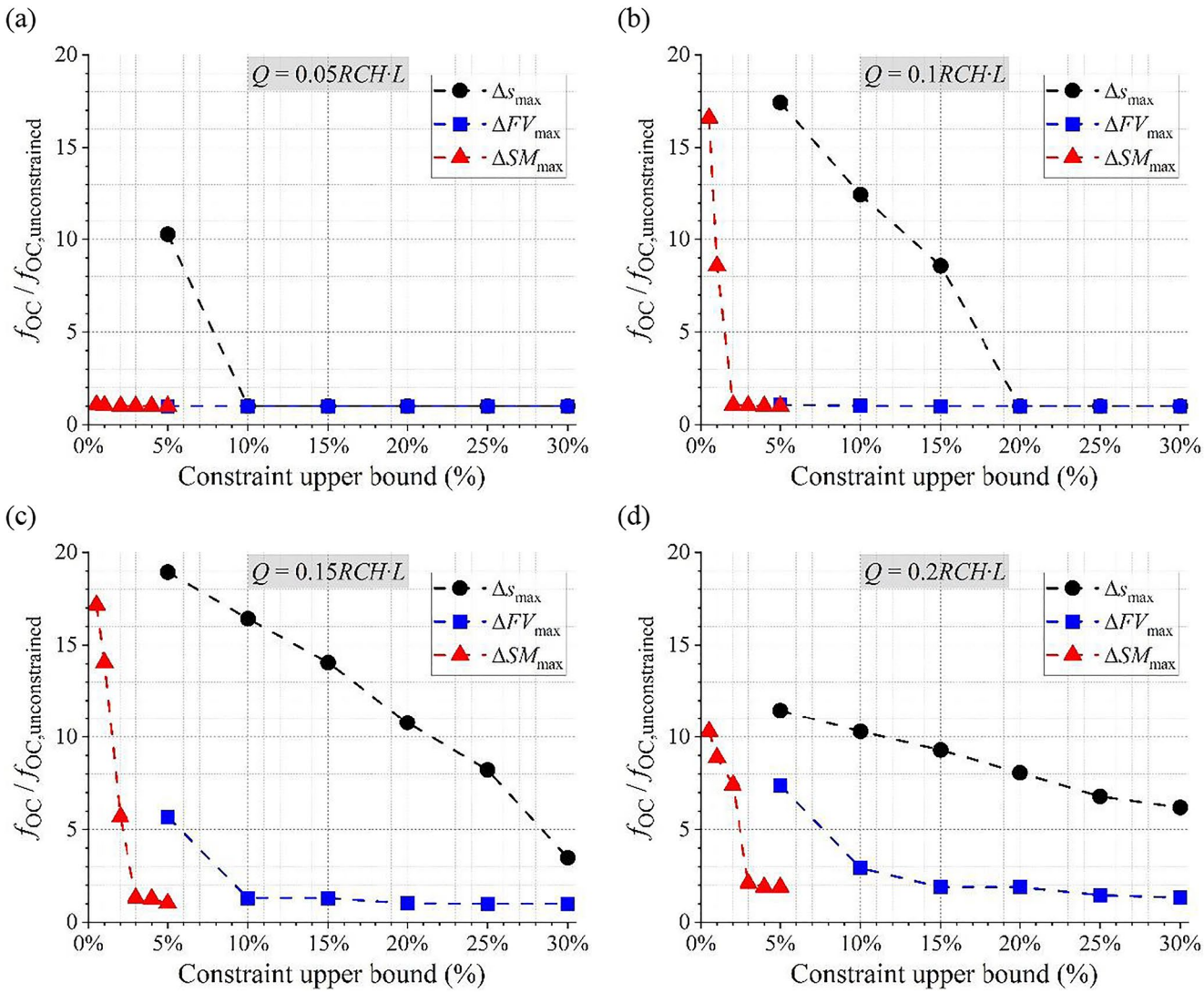

Figure 7. Trade-off profiles of the operation cost relative to unconstrained conditions versus the upper bounds Δs_{max}, ΔFV_{max}, and ΔSM_{max}, and for pumping rate ratios $Q/(\text{RCH} \cdot L)$ equal to (a) 0.05, (b) 0.1, (c) 0.15, and (d) 0.2.

3.3. Groundwater Management Under Single SWI Constraint Scenarios

To investigate the impact of the constraints, Δs (Equation 8), ΔFV (Equation 10) and ΔSM (Equation 12), each constraint is first imposed separately. The cost-optimal pumping strategies determined by these constraints are thus selected and compared for progressively increasing (i.e., less stringent) values of the upper bounds Δs_{max}, ΔFV_{max}, and ΔSM_{max}, as indicated in Table 3. For each scenario, the identification of the optimal pumping strategy requires first to determine the feasible set of pumping schemes that meet the considered SWI constraint among the pool of 224 SEAWAT model runs, and then to identify the strategy with the minimum f_{OC} value. The results of this analysis are presented in Figures 7 and 8.

Figure 7 shows profiles of the minimum operation cost under variable SWI constraints and pumping rate normalized by the recharge, that is, $Q/(\text{RCH} \cdot L)$. In each subpanel, the cost is scaled with respect to the cost under unconstrained conditions, that is, optimal-cost values calculated by imposing no limitations on SWI indicators. The unconstrained cost values, $f_{OC,u}$, are 0.50, 1.04, 1.61, and 3.71 \$/(m · year) for pumping rate ratios of 0.05, 0.1, 0.15 and 0.2, respectively.

The profiles in Figure 7 illustrate the tradeoffs existing between the management cost and the stringency of the SWI constraints adopted. It is worth observing that for low pumping rates (Figures 7a and 7b), the optimal cost

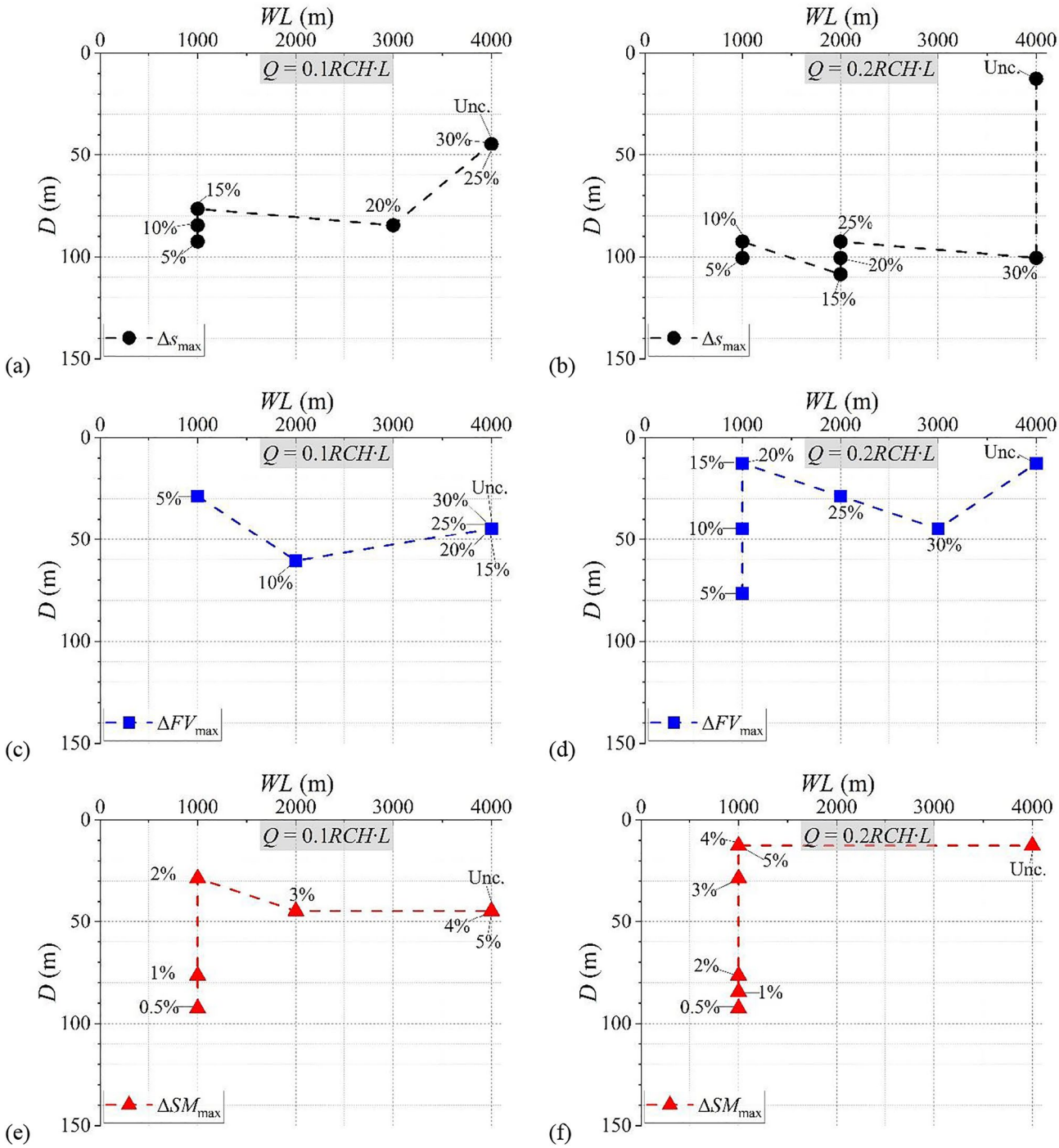

Figure 8. Representation of the location of the pumping system under the tradeoff profiles shown in Figure 7, for variable constraint scenarios for (a, b) Δs_{max}, (c, d) ΔFV_{max} and (e, f) ΔSM_{max}, and for pumping rate ratios $Q/(\text{RCH} \cdot L)$ equal to 0.1, and 0.2. Percentages represent the upper bounds of employed constraints while "Unc." denotes the unconstrained case.

may result in the same as in the unconstrained case (i.e., $f_{OC}/f_{OC,u} = 1$) when the constraint bound is large enough for the constraint to be "non-binding." Regardless of the selected pumping rate Q, the increase in cost due to the constraint is generally more pronounced in relation to Δs_{max}, followed by ΔSM_{max}, and then by ΔFV_{max}, at least within the intervals of variability considered for these upper bounds (Table 3). Figure 7 shows that the relative cost $f_{OC}/f_{OC,u}$ is larger for $Q/(\text{RCH} \cdot L)$ values of 0.1 (subpanel b) and 0.15 (subpanel c), than for 0.2 (subpanel

d), which reveals that the specific (per unit volume) cost of groundwater supply is a nonlinear function of the pumping rate. A detailed analysis of these effects is provided in Appendix C.

Figure 8 provides a representation of the cost-optimal pumping schemes identified in the tradeoff profiles in Figure 7 for pumping rate ratios $Q/(\text{RCH} \cdot L)$ equal to 0.1 (subpanels 8a, 8c, and 8e) and 0.2 (subpanels 8b, 8d, and 8f). In all subpanels, the unconstrained solution is also shown, which indicates that, with no SWI constraint, the pumping system should be positioned at the island center ($WL = 0.5 \cdot L$), and at a depth D that decreases with increasing Q.

Figures 8a and 8b show that when the SWI constraint (7) is made more stringent, that is, the bound for $\Delta s_{\max}$ is reduced, and the pumping rate Q is increased, the pumping system optimal location tends to shift first to a larger depth and then closer to the shoreline. As seen in Figure 7, this has a strong impact on the management cost since it strongly increases the need for desalination treatment. A quite different "pathway" is observed in Figures 8c and 8d. For $Q/(\text{RCH} \cdot L)$ equal to 0.1, where the optimal pumping location shifts from a larger depth around the center of the island, to a shallower depth closer to the shoreline as the SWI constraint (9) is progressively tightened. A similar behavior is observed for $Q/(\text{RCH} \cdot L)$ equal to 0.2, but when the constraint is most stringent, the optimal pumping location is found closer to the shoreline and at a larger depth. This shows that to limit ΔFV, it is necessary to abstract groundwater at the fringes of the freshwater lens, where the water salinity if higher. Figures 8e and 8f exhibit some analogies with Figures 8c and 8d. If $Q/(\text{RCH} \cdot L) = 0.2$ and $\Delta SM_{\max}$ is set to 5%, or less, all cost-optimal pumping schemes are found near the shoreline, and at a depth D that increases with the pumping rate Q. In practice, to strongly limit ΔSM, it is convenient to extract water in regions of the aquifer where salinity is higher, that is, at the lateral and deeper fringes of the freshwater lens.

These results underline that different SWI constraint indicators lead generally to the selection of quite different pumping schemes. As observed in the Δs, ΔFV, and ΔSM profiles presented in Figures 6 and 7, SWI constraints on Δs lead to more centered and deeper pumping systems, whereas SWI constraints on ΔFV and/or ΔSM lead to relatively shallower pumping systems positioned toward the shoreline. The former are relatively more expensive than the latter, as they tend to produce groundwater with higher salt concentration, which has higher desalination requirements.

3.4. Investigation of Optimal Pumping Strategies Under Multiple SWI Constraints

This section investigates the solutions to the management problem subject to multiple SWI constraints. For each constraint indicator, three threshold values of $\Delta s_{\max}$, $\Delta FV_{\max}$, and $\Delta SM_{\max}$ are investigated. For combinations of two SWI constraints 12 scenarios are considered (Table 4), and for combinations of three SWI constraints 8 scenarios are considered (Table 5). Tables 6 and 7 summarize the cost-optimal management schemes under two and three concurrent SWI constraints, respectively.

In Table 6, Scenarios 1–4 report optimal cost values subject to concurrent constraints on Δs and ΔFV (inequalities 7 and 9). It is observed that constraints are generally non-binding if $Q = 0.05 \cdot \text{RCH} \cdot L$, and may affect the cost only for larger pumping rates. In these instances, for smaller values of $\Delta s_{\max}$ (10%), the constraint (7) is "binding," that is, satisfied with equality at the optimal solution ($\Delta s = \Delta s_{\max}$), whereas constraint (9) has no impact on the optimal cost (i.e., $\Delta FV < \Delta FV_{\max}$). Indeed, it should be noticed that if the optimal solution is driven exclusively by one constraint (e.g., Scenario 1), then any other scenario in which the other constraint bound is increased (e.g., Scenario 2) will provide the same optimal solution. For larger values of $\Delta s_{\max}$ (30%), constraint (9) is binding and affects the optimal cost jointly with constraint (7) if $\Delta FV_{\max}$ is set to 10% (Scenario 3) but has otherwise no impact if this is relaxed to 30% (Scenario 4).

Scenarios 5–8 report the optimal f_{OC} in the presence of constraints on Δs and ΔSM (inequalities 7 and 11). For $Q = 0.05 \cdot \text{RCH} \cdot L$, the optimal cost is affected only when $\Delta SM_{\max}$ is set to 1% (Scenarios 5 and 7), otherwise, the optimal solution is the unconstrained, that is, the constraints result in non-binding. For larger values of Q, some of the SWI constraints may have an impact on the optimal cost. For example, for smaller values of $\Delta s_{\max}$ (10%), the constraint (7) results in binding (Scenarios 5 and 6), and for $Q = 0.15 \cdot \text{RCH} \cdot L$, it affects the optimal cost jointly with constraint (11) if $\Delta SM_{\max} = 1\%$. For larger values of $\Delta s_{\max}$ (30%), constraint (11) has an impact on the cost only if $\Delta SM_{\max}$ is set to 1% (Scenario 7). If $\Delta SM_{\max}$ equals 5%, the optimal cost depends only on the constraint (7) (Scenario 8).

Table 6
Optimal f_{OC} Under the Different Combinations of Two Types of Constraint Conditions

Scenario	Δs_{max} (7)	ΔFV_{max} (9)	ΔSM_{max} (11)	Optimal f_{OC} ($/(m · year)) $\frac{Q}{RCH \cdot L} = 0.05$	$\frac{Q}{RCH \cdot L} = 0.1$	$\frac{Q}{RCH \cdot L} = 0.15$	$\frac{Q}{RCH \cdot L} = 0.2$
1	10%	10%	–	$0.50^{(U)}$	$12.91^{(7)}$	$26.36^{(7)}$	$38.17^{(7)}$
2	10%	30%	–	$0.50^{(U)}$	$12.91^{(7)}$	$26.36^{(7)}$	$38.17^{(7)}$
3	30%	10%	–	$0.50^{(U)}$	$1.06^{(9)}$	$9.13^{(7–9)}$	$25.15^{(7–9)}$
4	30%	30%	–	$0.50^{(U)}$	$1.04^{(U)}$	$5.59^{(7)}$	$22.93^{(7)}$
5	10%	–	1%	$0.52^{(11)}$	$12.91^{(7)}$	$27.54^{(7–11)}$	$38.17^{(7)}$
6	10%	–	5%	$0.50^{(U)}$	$12.91^{(7)}$	$26.36^{(7)}$	$38.17^{(7)}$
7	30%	–	1%	$0.52^{(11)}$	$8.88^{(11)}$	$22.56^{(11)}$	$32.94^{(11)}$
8	30%	–	5%	$0.50^{(U)}$	$1.04^{(U)}$	$5.59^{(7)}$	$22.93^{(7)}$
9	–	10%	1%	$0.52^{(11)}$	$8.88^{(11)}$	$22.56^{(11)}$	$32.94^{(11)}$
10	–	10%	5%	$0.50^{(U)}$	$1.06^{(9)}$	$2.09^{(9)}$	$10.83^{(9)}$
11	–	30%	1%	$0.52^{(11)}$	$8.88^{(11)}$	$22.56^{(11)}$	$32.94^{(11)}$
12	–	30%	5%	$0.50^{(U)}$	$1.04^{(U)}$	$1.64^{(11)}$	$7.02^{(11)}$

Note. Cost values are provided with a superscript that represents the seawater intrusion constraints that result binding for the optimal pumping scheme (e.g., "(7)" for constraint (7), "(7–9)" for constraints (7) and (9)). The "(U)" superscript denotes conditions in which none of the constraints is binding. The symbol "–" indicates an inactive constraint.

Scenarios 9–12 report optimal f_{OC} values subject to joint constraints on ΔFV and ΔSM (inequalities 9 and 11). Although constraints result generally non-binding if Q is equal to $0.05 \cdot RCH \cdot L$, and affect the management cost only for larger pumping rates, it is observed that the constraint (11) results in binding if ΔSM_{max} is set equal to 1% (Scenarios 9 and 11). For lower values of ΔFV_{max} (10%), constraint (9) results in non-binding when ΔSM_{max} is equal to 1% (Scenario 9) and binding if ΔSM_{max} is equal to 5% (Scenario 10). Finally, for larger values of ΔFV_{max} (30%), constraint (9) does not affect the cost, which depends only on the constraint (11), that is, ΔSM_{max} (Scenarios 11–12).

Table 6 reveals that, in most scenarios, the optimal f_{OC} and the corresponding feasible pumping scheme under two types of SWI constraints primarily hinge upon one dominant constraint, while the other remains ineffective. There exist, however, combinations of SWI constraints that result in joint binding of constraints (Scenarios 3 and 5). In these situations, the optimal solution needs to be "conservatively" within the intersection of the feasibility sets associated with the single constraints, which causes the minimum cost to increase.

Table 7 reports optimal cost values for the 12 combinations of the upper bounds Δs_{max}, ΔFV_{max} and ΔSM_{max} associated with the SWI constraints (7), (9), and (11), respectively. It can be noticed that for lower pumping rates, that is, $Q = 0.05 \cdot RCH \cdot L$, the constraints have an impact on the cost only if ΔSM_{max} is prescribed to be 1%, otherwise the unconstrained solution holds (Table 6). For pumping rates of $0.1 \cdot RCH \cdot L$, or larger, the optimal cost is consistently driven by the constraint (7) if Δs_{max} is set to 10% (Scenarios 13–16) and may also depend on the constraint (11) if ΔSM_{max} is set to 1% (Scenarios 13 and 15). For Δs_{max} equal to 30% (Scenarios 17–20), the constraint (11) is consistently dominant if ΔSM_{max} is set to 1% (Scenarios 17, 19). Otherwise, if ΔFV_{max} is set to 10%, the constraint (9) is binding (Scenario 18). In cases where ΔFV_{max} is set to 30% (Scenarios 19–20), the constraint (9) becomes non-binding, and the optimal cost depends either on constraints (7) or (11).

The comparison of the results in Tables 6 and 7, indicates that the scenarios limited by three types of constraint conditions often lead to the same optimal cost f_{OC} as those only constrained by only two of them. For example, the optimal strategies in Scenarios 13 and 15 are the same as those in Scenario 5, and Scenario 14 yields the same optimal solution as Scenarios 1 and 6. This shows that the optimal f_{OC} is still driven by a predominant constraint or jointly by two constraints, whereas the third constraint has no impact on the optimal pumping strategy. This can be generally attributed to the large upper bound for that constraint, which has little impact on the set of feasi-

Table 7
Optimal f_{OC} Under the Different Combinations of Three Types of Constraint Conditions

Scenario	Δs_{max} (7) (%)	ΔFV_{max} (9) (%)	ΔSM_{max} (11) (%)	Optimal f_{OC} ($/(m · year))			
				$\frac{Q}{RCH \cdot L} = 0.05$	$\frac{Q}{RCH \cdot L} = 0.1$	$\frac{Q}{RCH \cdot L} = 0.15$	$\frac{Q}{RCH \cdot L} = 0.2$
13	10	10	1	$0.52^{(11)}$	$12.91^{(7)}$	$27.54^{(7–11)}$	$38.17^{(7)}$
14	10	10	5	$0.50^{(U)}$	$12.91^{(7)}$	$26.36^{(7)}$	$38.17^{(7)}$
15	10	30	1	$0.52^{(11)}$	$12.91^{(7)}$	$27.54^{(7–11)}$	$38.17^{(7)}$
16	10	30	5	$0.50^{(U)}$	$12.91^{(7)}$	$26.36^{(7)}$	$38.17^{(7)}$
17	30	10	1	$0.52^{(11)}$	$8.88^{(11)}$	$22.56^{(11)}$	$32.94^{(11)}$
18	30	10	5	$0.50^{(U)}$	$1.06^{(9)}$	$9.13^{(7–9)}$	$25.15^{(7–9)}$
19	30	30	1	$0.52^{(11)}$	$8.88^{(11)}$	$22.56^{(11)}$	$32.94^{(11)}$
20	30	30	5	$0.50^{(U)}$	$1.04^{(U)}$	$5.59^{(7)}$	$22.93^{(7)}$

Note. Optimal f_{OC} values are provided with a superscript that represents the seawater intrusion constraints that result binding for the optimal pumping scheme (e.g., "(7)" for constraint (7), "(7–9)" for constraints (7) and (9)). The "(U)" superscript is used for the cost values in which none of the constraints is binding.

ble pumping schemes. In some instances, however, a constraint may reduce SWI in a similar mode to another constraint, so that adding it has a limited impact on the optimal solution.

It is finally worth remarking that, based on the profiles in Figures 6b–6d, (a) constraint (7) tends to exclude shallow pumping and select pumping wells deeper into the freshwater lens; (b) both constraints (9) and (11) tend to exclude pumping near the island center, and favor well locations closer to the shoreline. As shown in Figure 8, optimal solutions under the constraint $\Delta FV_{max} = 20\%$ are equivalent to those constrained with $\Delta SM_{max} = 5\%$. Likewise, both cost-optimal pumping strategies and the feasible pumping schemes are nearly the same with constraints $\Delta FV_{max} = 15\%$ and $\Delta SM_{max} = 4\%$. Therefore, the impact of constraint (9) on SWI control is practically equivalent to that of constraint (11). To reduce the complexity of management problems, the two constraints should not be adopted together. And if the SWI management is conducted with constraints on both Δs and ΔFV, the value of ΔFV_{max} needs to be small enough to affect the selection of a pumping strategy.

4. Conclusions

This study investigated the tradeoffs between the operational cost of groundwater supply and the sustainability of freshwater resources in island aquifers, considering a hydrogeological setting representative of San Salvador Island, Bahamas. Groundwater abstraction strategies have been characterized through three DVs, the distance WL from the shoreline, the pumping depth D, and the pumping rate Q. The analysis has relied on the formulation of an optimization problem, aiming to minimize the operation cost, given by the sum of the pumping cost and the desalination cost, subject to SWI constraints on aquifer drawdown above the pumping system, Δs, decrease of freshwater volume, ΔFV, and increase in salt mass within the aquifer, ΔSM. The investigation has been based on the analysis of a large set of groundwater abstraction strategies, which has required as many as 224 steady-state SEAWAT model runs to calculate the optimal operation cost and the corresponding constraint variables.

Our investigation demonstrated that, in general, pumping at larger depth D leads to a reduced drawdown Δs, but also to an increased salt concentration C in the abstracted groundwater. As both the water table elevation and the freshwater lens thickness under natural conditions increase toward the island center, pumping schemes with increasing WL lead to an increased aquifer drawdown Δs and to a reduced salt concentration C. Accordingly, for any given Q and D, placing the pumping well system toward the island center represents the best strategy to minimize the operation cost.

However, the formulated SWI indicators show that pumping in proximity of the island center has a negative impact on the availability of freshwater resources in the aquifer, when compared to the effect of "decentralized" pumping strategies. This highlights an inherent conflict between SWI control and the economic cost of groundwater supply. When Q is a small fraction of the natural groundwater recharge, pumping does not

violate limitations on SWI, and the optimal pumping strategy is the same as under unconstrained conditions. However, if Q is increased or constraints on SWI are tightened, the optimal pumping strategies are characterized by larger pumping depth values and smaller distances from the shoreline to limit SWI, leading to higher operation costs.

In terms of SWI control, the impact of constraints on Δs on cost-optimal pumping strategies is quite different than that of constraints on ΔFV and ΔSM. Constraints on Δs are observed to lead to selecting deeper pumping systems located towards the island center, whereas both the constraints on ΔFV and ΔSM favor the choice of shallower pumping systems closer to the shoreline. As a result, the pumping strategies under Δs constraints are generally more expensive than those under ΔFV and ΔSM constraints, as they involve the extraction of groundwater with higher salinity that requires more intense desalination treatment.

When the investigated SWI constraints are imposed concurrently, optimal pumping strategies are often driven by the most stringent of them. However, there may exist combinations of SWI bounds in which the most cost-effective pumping strategy depends jointly on more constraints, in which case the groundwater supply cost is higher than it would be if either constraint was selected separately. Our analysis has shown also that constraints on ΔFV and ΔSM exhibit a practical equivalence in terms of SWI control, and to reduce the complexity of management problems, they should not be adopted simultaneously in the optimization formulation of the groundwater management problem.

One needs to be aware of potential limitations in the methods adopted in this study. First, the operation cost of groundwater supply is assumed to be driven exclusively by the energy required for the pumping and the desalination of groundwater by RO but does not account for other processes of water resource management, for example, brine disposal, water distribution and wastewater treatment. While the economic impact of processes that have been overlooked may be significant, the cost of groundwater desalination typically constitutes the most important component on which groundwater management depends, and this provides a firm basis for the transferability of the results of this study to the most common island aquifer settings.

In this paper, we focused on exploring the trade-offs between the operation cost of groundwater supply and different formulations of SWI constraints using a simplified 2D representation. Although we are aware that a 2D model may not fully capture the complexity of real-world 3D systems with multiple pumping wells, we intentionally chose this approach to ensure computational viability and feasibility within the scope of our study. We simplified the pumping system by conceptualizing it as a horizontal sink, assuming uniform distribution of groundwater abstraction along it. While this approach may underestimate aquifer drawdown in individual wells, it allowed us to consider fewer DVs and conduct a reasonably simplified analysis on management cost and constraint formulation. As a result, our findings are intended to be generic to island aquifers, even though they are based on the general characteristics of a specific site. As such, this analysis serves as a crucial initial step towards developing more sophisticated models that can effectively address the optimization challenges associated with groundwater management in real-world island aquifers, such as the one of San Salvador Island.

Appendix A: Energy Consumption for Water Desalination by Reverse-Osmosis

As RO is the most popular technique for desalinating brackish water and seawater in coastal groundwater management (Abd-Elhamid & Javadi, 2011; Hussain et al., 2019), it is the method considered in this work to treat groundwater whose salt concentration exceeds accepted potability standards. The specific (per unit mass) energy consumption for desalination SEC [L^2T^{-2}] by RO is estimated as (Stillwell & Webber, 2016):

$$\mathrm{SEC}(C) = \frac{R \cdot T_s}{M_w} \cdot \left\{ \frac{x_{s\mathrm{F}} - x_{s\mathrm{P}}}{x_{s\mathrm{B}} - x_{s\mathrm{F}}} \cdot \left[x_{s\mathrm{B}} \cdot \ln\left(\frac{x_{s\mathrm{B}}}{x_{s\mathrm{F}}}\right) + x_{w\mathrm{B}} \cdot \ln\left(\frac{x_{w\mathrm{B}}}{x_{w\mathrm{F}}}\right) \right] + \left[x_{s\mathrm{P}} \cdot \ln\left(\frac{x_{s\mathrm{P}}}{x_{s\mathrm{F}}}\right) + x_{w\mathrm{P}} \cdot \ln\left(\frac{x_{w\mathrm{P}}}{x_{w\mathrm{F}}}\right) \right] \right\} \tag{A1}$$

where R is the universal gas constant, T_s is the saturation absolute temperature [K], and M_w is the water molecular weight [for example, M/mole]. The symbols x represents mole fractions [/], with the subscripts "s" and "w" referring to salt and water, respectively. The subscript F indicates the "feed," that is, the water abstracted

that undergoes desalination; the subscript P stands for "permeate," that is, the water distributed to users after desalination; and the subscript B denotes "brine," that is, the by-product high salinity water produced by RO, which is typically disposed.

The salt mole fraction of the feed, $x_{s\mathrm{F}}$, can be calculated from the feed water concentration C as (Avlonitis et al., 2012):

$$x_{s\mathrm{F}} = \frac{C/M_s}{C/M_s + [\rho_w(C) - C]/M_w} \tag{A2}$$

where M_s is the salt molecular weight [M/mole]. The water mole fraction of the feed $x_{w\mathrm{F}}$ is:

$$x_{w\mathrm{F}} = 1 - x_{s\mathrm{F}} \tag{A3}$$

The mole fractions of the permeate, $x_{s\mathrm{P}}$ and $x_{w\mathrm{P}}$, are obtained using Equations A2 and A3 with C equal to the target concentration C_d in the permeate, assumed to be 1.0 g/L. Likewise, the mole fractions for the brine, $x_{s\mathrm{B}}$ and $x_{w\mathrm{B}}$, are calculated using Equations A2 and A3, with C equal to the brine concentration C_b, whose value varies depending on the adopted desalination system. If this is designed to provide a fixed recovery ratio r between the flow rate Q_d sent to water users and the feed flow rate Q ($r = Q_d/Q$), then the brine mole fractions can be derived by combining the mass balance equations of water and salt for the treatment plant (Avlonitis et al., 2012):

$$x_{\mathrm{sB}} = \frac{x_{s\mathrm{F}} - r x_{s\mathrm{P}}}{1 - r} \tag{A4}$$

$$x_{\mathrm{wB}} = \frac{1 - x_{s\mathrm{F}} - r x_{w\mathrm{P}}}{1 - r} \tag{A5}$$

The resulting brine concentration can then be calculated as:

$$C_b = \frac{1}{1 - r} \cdot C - \frac{r}{1 - r} \cdot C_d \tag{A6}$$

Equation A6 shows that C_b may result excessively large for high recovery ratios (e.g., $r > 0.8$) and large feed concentrations C, which ultimately leads to cost-ineffective energy consumption (Squire, 2000). On the other hand, if the feed concentration C is slightly above the target C_d, large quantities of brine with relatively low concentration are discarded, which may result cost-ineffective as well.

If the desalination system is designed to achieve a fixed brine concentration C_b, Equations A2 and A3 with $C = C_b$ are still valid, but the recovery ratio r results a function of the feed concentrations C, which is obtained from Equation A6 as:

$$r = \frac{C_b - C}{C_b - C_d} \tag{A7}$$

In this work, we adopt the latter approach and select a fixed brine concentration value C_b of 150.0 g/L (Ahunbay, 2019; Azerrad et al., 2019). For $C_d = 1$ g/L, and C ranging from 1 to 35 g/L, r values vary between 0.77 and 1 (Equation A7).

Appendix B: Pump Costs Associated With Various Pumping Intensities

To distinguish the effects of DVs on f_p, Figure B1 presents the profiles of f_p for Q values equal to $0.05\mathrm{RCH} \cdot L$ (subpanel B1a), $0.1\mathrm{RCH} \cdot L$ (subpanel B1b), $0.15\mathrm{RCH} \cdot L$ (subpanel B1c) and $0.2\mathrm{RCH} \cdot L$ (subpanel B1d). In general, the pumping cost f_p is larger if the pumping rate Q increases, and smaller if WL increases. These profiles show that with the pumping depth D increasing, f_p first drops slightly before increasing dramatically and then

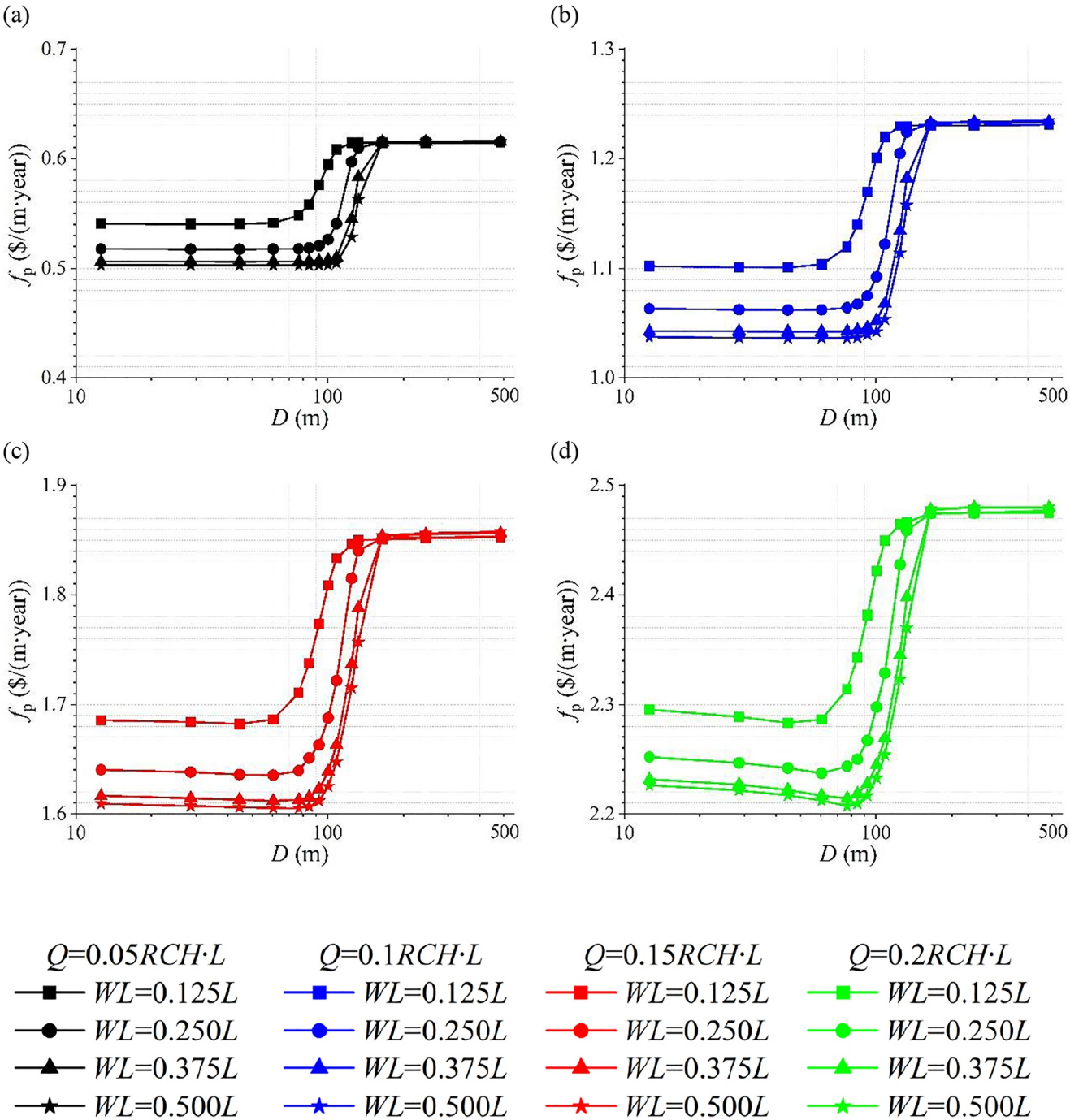

Figure B1. Profiles of f_p under variable Q for (a) 0.05RCH · L, (b) 0.1RCH · L, (c) 0.15RCH · L and (d) 0.2RCH · L.

keeps nearly constant. The behavior of f_p reducing at the lower D, between 12.6 and ~100 m, becomes more obvious with Q increasing (e.g., Figures B1c and B1d). These trends are explained by observing the behavior of h in the DV space (D, WL, Q), as shown in Figure 5a, and noting the dependency of f_p on h and Q in Equation 2.

Appendix C: Cost Per Unit Water Under Variable Constraint Scenarios

It is worth highlighting that, in Figure 7, since the overall groundwater supply cost increases nonlinearly depending on the stringency of the adopted SWI constraints, and since the recovery ratio r (Equation A7) depends on the

solute concentration C, the cost per unit water volume delivered to users, that is, $\overline{f}_{OC} = f_{OC}/(r \cdot Q)$ (\$/m^3), results a complex nonlinear function of constraint bounds Δs_{max}, ΔFV_{max} and ΔSM_{max}.

Figure C1 presents the profiles of $\overline{f}_{OC}$ calculated for each selected Q and for variable constraint bounds Δs_{max} (subpanel C1a), ΔFV_{max} (subpanel C1b) and ΔSM_{max} (subpanel C1c). These profiles show that, for any given Q, the optimal $\overline{f}_{OC}$ generally increases from unconstrained conditions to more and more stringent SWI bounds Δs_{max}, ΔFV_{max} and ΔSM_{max}. For smaller values of Q, the set constraints result in non-binding and $\overline{f}_{OC}$ remains the same as in the unconstrained case. However, if the SWI bounds are prescribed below a certain threshold, then the constraints become binding and the optimal pumping strategy inevitably involves the abstraction of groundwater with a salt concentration C that requires treatment, which has a major impact on f_{OC} (Equation 3) and also implies a reduced recovery ratio r (Equation A7), which further increases $\overline{f}_{OC}$. Comparison of the profiles in Figures C1a, C1b, and C1c also confirm that $\overline{f}_{OC}$ is generally more sensitive to constraints on Δs, than it is to constraints on ΔSM, or ΔFV.

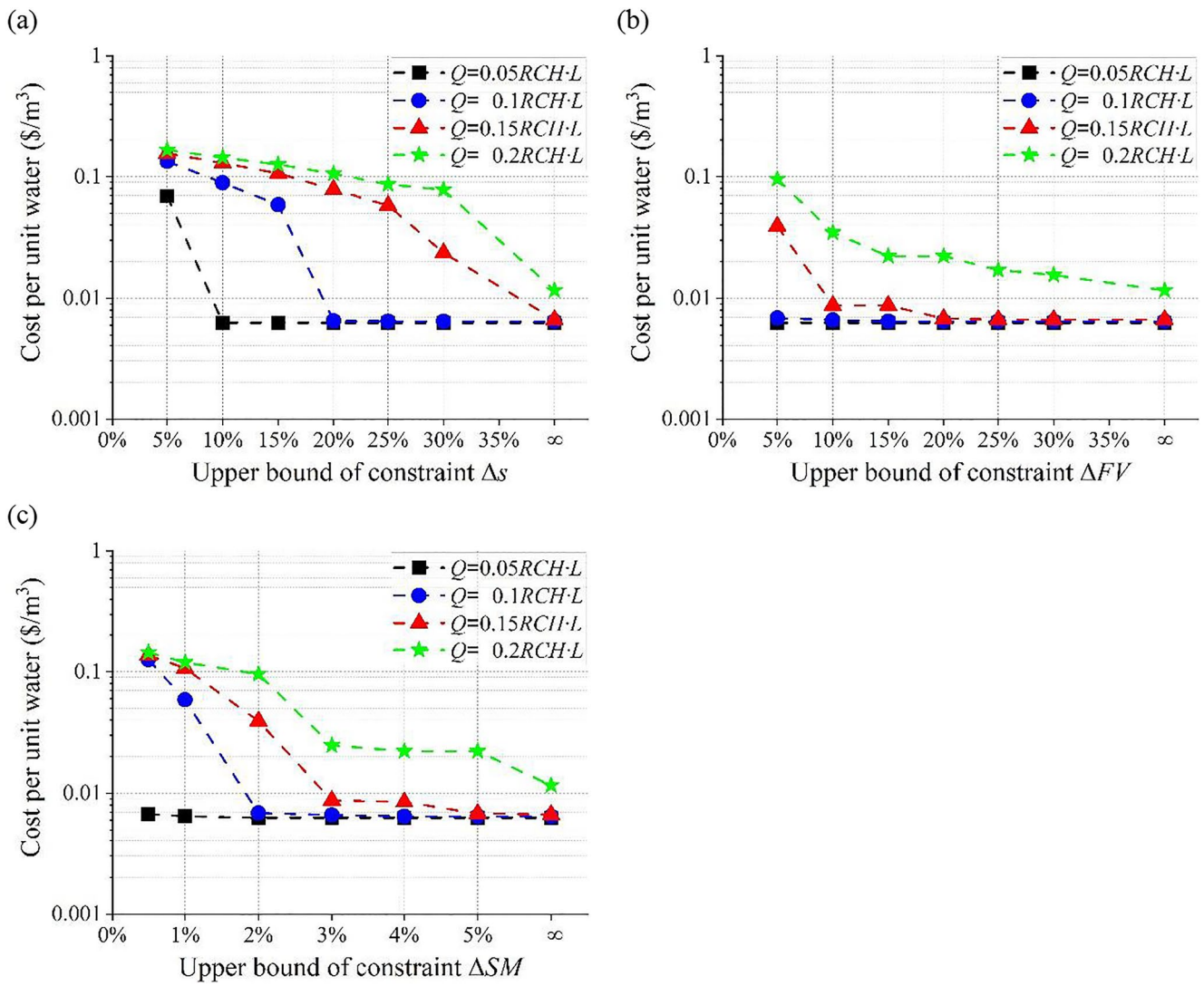

Figure C1. Profiles of the cost per unit water delivered as a function of Q under variable constraint scenarios for (a) Δs_{max}, (b) ΔFV_{max} and (c) ΔSM_{max}.

Data Availability Statement

Data—The input file for modeling SWI in the 2D simplified San Salvador Island aquifer can be found in Yu et al. (2023).

Software—Salinity distribution in the island aquifer during pumping was simulated using version 4 of the SEAWAT groundwater software (United States Geological Survey, 2012).

Acknowledgments

The authors have no relevant financial or non-financial interests to declare that are relevant to the content of this article. This work was partially supported by the EPSRC Grant EP/T018542/1, and the NSF under grant agreement CBET-EPSRC 2022278. The authors also would like to thank the editor, Dr. Georgios Kourakos and two other anonymous reviewers for their kind feedback and insightful comments, which helped improve the clarity of this paper.

References

Abd-Elhamid, H. F., & Javadi, A. A. (2011). A cost-effective method to control seawater intrusion in coastal aquifers. *Water Resources Management*, *25*(11), 2755–2780. https://doi.org/10.1007/s11269-011-9837-7

Abdoulhalik, A., Ahmed, A., & Hamill, G. A. (2017). A new physical barrier system for seawater intrusion control. *Journal of Hydrology*, *549*, 416–427. https://doi.org/10.1016/j.jhydrol.2017.04.005

Agoubi, B. (2021). A review: Saltwater intrusion in North Africa's coastal areas-current state and future challenges. *Environmental Science and Pollution Research*, *8*(14), 17029–17043. https://doi.org/10.1007/s11356-021-12741-z

Ahunbay, M. G. (2019). Achieving high water recovery at low pressure in reverse osmosis processes for seawater desalination. *Desalination*, *465*, 58–68. https://doi.org/10.1016/j.desal.2019.04.023

Avlonitis, S. A., Avlonitis, D. A., & Panagiotidis, T. (2012). Experimental study of the specific energy consumption for brackish water desalination by reverse osmosis. *International Journal of Energy Research*, *36*(1), 36–45. https://doi.org/10.1002/er.1780

Azerrad, S. P., Isaacs, M., & Dosoretz, C. G. (2019). Integrated treatment of reverse osmosis brines coupling electrocoagulation with advanced oxidation processes. *Chemical Engineering Journal*, *356*, 771–780. https://doi.org/10.1016/j.cej.2018.09.068

Baù, D. A., & Mayer, A. S. (2006). Stochastic management of pump-and-treat strategies using surrogate functions. *Advances in Water Resources*, *29*(12), 1901–1917. https://doi.org/10.1016/j.advwatres.2006.01.008

Beheshti, J., Javadi, S., Hosseini, S. A., & Moghaddam, H. K. (2022). Evaluation of strategies for pumping optimization of coastal aquifers using numerical simulation and game theory. *Environmental Earth Sciences*, *81*(12), 340. https://doi.org/10.1007/s12665-022-10459-w

Botero-Acosta, A., & Donado, L. D. (2015). Laboratory scale simulation of hydraulic barriers to seawater intrusion in confined coastal aquifers considering the effects of stratification. *Procedia Environmental Sciences*, *25*, 36–43. https://doi.org/10.1016/j.proenv.2015.04.006

Bray, B. S., & Yeh, W. W. G. (2008). Improving seawater barrier operation with simulation optimization in southern California. *Journal of Water Resources Planning and Management*, *134*(2), 171–180. https://doi.org/10.1061/(ASCE)0733-9496(2008)134:2(171)

Christelis, V., & Mantoglou, A. (2016). Pumping optimization of coastal aquifers assisted by adaptive metamodelling methods and radial basis functions. *Water Resources Management*, *30*(15), 5845–5859. https://doi.org/10.1007/s11269-016-1337-3

Christelis, V., & Mantoglou, A. (2019). Pumping optimization of coastal aquifers using seawater intrusion models of variable-fidelity and evolutionary algorithms. *Water Resources Management*, *33*(2), 555–568. https://doi.org/10.1007/s11269-018-2116-0

Coulon, C., Lemieux, J.-M., Pryet, A., Bayer, P., Young, N. L., & Molson, J. (2022). Pumping optimization under uncertainty in an island freshwater lens using a sharp-interface seawater intrusion model. *Water Resources Research*, *58*(8), e2021WR031793. https://doi.org/10.1029/2021WR031793

Davis, R. L., & Johnson, C. R. (1989). Karst hydrology of San Salvador. In J. E. Mylroie (Ed.), *Proceedings of the fourth symposium on the geology of the Bahamas. Bahamian Field Station, San Salvador Island, Bahamas* (pp. 118–135).

Dey, S., & Prakash, O. (2020). Managing saltwater intrusion using conjugate sharp interface and density dependent models linked with pumping optimization. *Groundwater for Sustainable Development*, *11*, 100446. https://doi.org/10.1016/j.gsd.2020.100446

El-Ghandour, H. A., & Elbeltagi, E. (2020). Pumping optimization of coastal aquifers using probabilistic search – Case study: Quaternary aquifer of El-Arish Rafah, Egypt. *Hydrology Research*, *51*(1), 90–104. https://doi.org/10.2166/nh.2019.093

Fan, Y., Lu, W., Miao, T., Li, J., & Lin, J. (2020). Multiobjective optimization of the groundwater exploitation layout in coastal areas based on multiple surrogate models. *Environmental Science and Pollution Research*, *27*(16), 19561–19576. https://doi.org/10.1007/s11356-020-08367-2

Ferreira da Silva, J. F., & Haie, N. (2007). Optimal locations of groundwater extractions in coastal aquifers. *Water Resources Management*, *21*(8), 1299–1311. https://doi.org/10.1007/s11269-006-9082-7

Fetter, C. W. (1972). Position of the saline water interface beneath oceanic islands. *Water Resources Research*, *8*(5), 1307–1315. https://doi.org/10.1029/WR008i005p01307

Gulley, J. D., Mayer, A. S., Martin, J. B., & Bedekar, V. (2016). Sea level rise and inundation of island interiors: Assessing impacts of lake formation and evaporation on water resources in arid climates. *Geophysical Research Letters*, *43*(18), 9712–9719. https://doi.org/10.1002/2016GL070667

Ho, H. C., Mylroie, J. E., Infante, L. R., & Rodgers, J. C. (2014). Fuzzy-based spatial modeling approach to predict island karst distribution: A conceptual model. *Environmental Earth Sciences*, *71*(3), 1369–1377. https://doi.org/10.1007/s12665-013-2543-4

Holding, S., & Allen, D. M. (2015). From days to decades: Numerical modelling of freshwater lens response to climate change stressors on small low-lying islands. *Hydrology and Earth System Sciences*, *19*(2), 933–949. https://doi.org/10.5194/hess-19-933-2015

Hussain, M. S., Abd-Elhamid, H. F., Javadi, A. A., & Sherif, M. M. (2019). Management of seawater intrusion in coastal aquifers: A review. *Water*, *11*(12), 2467. https://doi.org/10.3390/w11122467

Jakovovic, D., Post, V. E. A., Werner, A. D., Männicke, O., Hutson, J. L., & Simmons, C. T. (2011). Tracer adsorption in sand-tank experiments of saltwater up-coning. *Journal of Hydrology*, *414–415*, 476–481. https://doi.org/10.1016/j.jhydrol.2011.11.024

Jasechko, S., Perrone, D., Seybold, H., Fan, Y., & Kirchner, J. W. (2020). Groundwater level observations in 250,000 coastal US wells reveal scope of potential seawater intrusion. *Nature Communications*, *11*(1), 3229. https://doi.org/10.1038/s41467-020-17038-2

Javadi, A. A., Abd-Elhamid, H. F., & Farmani, R. (2012). A simulation-optimization model to control seawater intrusion in coastal aquifers using abstraction/recharge wells. *International Journal for Numerical and Analytical Methods in Geomechanics*, *36*(16), 1757–1779. https://doi.org/10.1002/nag.1068

Javadi, A. A., Hussain, M., Sherif, M., & Farmani, R. (2015). Multi-objective optimization of different management scenarios to control seawater intrusion in coastal aquifers. *Water Resources Management*, *29*(6), 1843–1857. https://doi.org/10.1007/s11269-015-0914-1

Karatzas, G. P., & Dokou, Z. (2015). Optimal management of saltwater intrusion in the coastal aquifer of Malia, Crete (Greece), using particle swarm optimization. *Hydrogeology Journal*, *23*(6), 1181–1194. https://doi.org/10.1007/s10040-015-1286-6

Kazakis, N., Spiliotis, M., Voudouris, K., Pliakas, F. K., & Papadopoulos, B. (2018). A fuzzy multicriteria categorization of the GALDIT method to assess seawater intrusion vulnerability of coastal aquifers. *Science of the Total Environment*, *621*, 524–534. https://doi.org/10.1016/j.scitotenv.2017.11.235

Ketabchi, H., & Ataie-Ashtiani, B. (2015). Evolutionary algorithms for the optimal management of coastal groundwater: A comparative study toward future challenges. *Journal of Hydrology*, *520*, 193–213. https://doi.org/10.1016/j.jhydrol.2014.11.043

Kishi, Y., & Fukuo, Y. (1977). Studies on salinization of groundwater, I: Theoretical consideration on the three-dimensional movement of the salt water interface caused by the pumpage of confined groundwater in fan-shaped alluvium. *Journal of Hydrology*, *35*(1), 1–29. https://doi.org/10.1016/0022-1694(77)90074-9

Kopsiaftis, G., Christelis, V., & Mantoglou, A. (2019). Comparison of sharp interface to variable density models in pumping optimisation of coastal aquifers. *Water Resources Management*, *33*(4), 1397–1409. https://doi.org/10.1007/s11269-019-2194-7

Kourakos, G., & Mantoglou, A. (2011). Simulation and multi-objective management of coastal aquifers in semi-arid regions. *Water Resources Management*, *25*(4), 1063–1074. https://doi.org/10.1007/s11269-010-9677-x

Kourakos, G., & Mantoglou, A. (2013). Development of a multi-objective optimization algorithm using surrogate models for coastal aquifer management. *Journal of Hydrology*, *479*, 13–23. https://doi.org/10.1016/j.jhydrol.2012.10.050

Kourakos, G., & Mantoglou, A. (2015). An efficient simulation-optimization coupling for management of coastal aquifers. *Hydrogeology Journal*, *23*(6), 1167–1179. https://doi.org/10.1007/s10040-015-1293-7

Langevin, C. D., Thorne, D. T., Jr. Dausman, A. M., Sukop, M. C., & Guo, W. (2007). SEAWAT Version 4: A computer program for simulation of multi-species solute and heat transport. In *U.S. Geological Survey techniques and methods book 6* (p. 39). Chapter A22. https://doi.org/10.3133/tm6A22

Martin, J. B., & Moore, P. J. (2008). Sr concentrations and isotope ratios as tracers of ground-water circulation in carbonate platforms: Examples from San Salvador Island and Long Island, Bahamas. *Chemical Geology*, *249*(1), 52–65. https://doi.org/10.1016/j.chemgeo.2007.11.009

Mayer, A. S., Kelley, C. T., & Miller, C. T. (2002). Optimal design for problems involving flow and transport phenomena in saturated subsurface systems. *Advances in Water Resources*, *25*(8), 1233–1256. https://doi.org/10.1016/S0309-1708(02)00054-4

McGee, D. K., Wynn, J. G., Onac, B. P., Harries, P. J., & Rothfus, E. A. (2010). Tracing groundwater geochemistry using $\delta^{13}C$ on San Salvador Island (southeastern Bahamas): Implications for carbonate island hydrogeology and dissolution. *Carbonates and Evaporites*, *25*(2), 91–105. https://doi.org/10.1007/s13146-010-0013-6

McKinney, D. C., & Lin, M. D. (1994). Genetic algorithm solution of groundwater management models. *Water Resources Research*, *30*(6), 1897–1906. https://doi.org/10.1029/94WR00554

Moore, P. J. (2009). Controls on the generation of secondary porosity in eogenetic karst: Examples from San Salvador Island, Bahamas and north-central Florida, USA (Doctoral dissertation). University of Florida.

Motallebian, M., Ahmadia, H., Raoof, A., & Cartwright, N. (2019). An alternative approach to control saltwater intrusion in coastal aquifers using a freshwater surface recharge canal. *Journal of Contaminant Hydrology*, *222*, 56–64. https://doi.org/10.1016/j.jconhyd.2019.02.007

Park, N., & Shi, L. (2015). A comprehensive sharp-interface simulation-optimization model for fresh and saline groundwater management in coastal areas. *Hydrogeology Journal*, *23*(6), 1195–1204. https://doi.org/10.1007/s10040-015-1268-8

Pramada, S. K., Mohan, S., & Sreejith, P. K. (2018). Application of genetic algorithm for the groundwater management of a coastal aquifer. *ISH Journal of Hydraulic Engineering*, *24*(2), 124–130. https://doi.org/10.1080/09715010.2017.1378597

Qahman, K., Larabi, A., Ouazar, D., Naji, A., & Cheng, A. H. D. (2005). Optimal and sustainable extraction of groundwater in coastal aquifers. *Stochastic Environmental Research and Risk Assessment*, *19*(2), 99–110. https://doi.org/10.1007/s00477-004-0218-0

Rajabi, M. M., & Ketabchi, H. (2017). Uncertainty-based simulation-optimization using Gaussian process emulation: Application to coastal groundwater management. *Journal of Hydrology*, *555*, 518–534. https://doi.org/10.1016/j.jhydrol.2017.10.041

Ranjbar, A., & Mahjouri, N. (2019). Multi-objective freshwater management in coastal aquifers under uncertainty in hydraulic parameters. *Natural Resources Research*, *29*(4), 2347–2368. https://doi.org/10.1007/s11053-019-09585-3

Roy, D. K., & Datta, B. (2020). Modelling and management of saltwater intrusion in a coastal aquifer system: A regional-scale study. *Groundwater for Sustainable Development*, *11*, 100479. https://doi.org/10.1016/j.gsd.2020.100479

Roy, T., Schütze, N., Grundmann, J., Brettschneider, M., & Jain, A. (2016). Optimal groundwater management using state-space surrogate models: A case study for an arid coastal region. *Journal of Hydroinformatics*, *18*(4), 666–686. https://doi.org/10.2166/hydro.2016.086

Sedki, A., & Ouazar, D. (2011). Simulation-optimization modeling for sustainable groundwater development: A Moroccan Coastal aquifer case study. *Water Resources Management*, *25*(11), 2855–2875. https://doi.org/10.1007/s11269-011-9843-9

Song, J., Yang, Y., Wu, J., Wu, J., Sun, X., & Lin, J. (2018). Adaptive surrogate model based multiobjective optimization for coastal aquifer management. *Journal of Hydrology*, *561*, 98–111. https://doi.org/10.1016/j.jhydrol.2018.03.063

Squire, D. (2000). Reverse osmosis concentrate disposal in the UK. *Desalination*, *132*(1), 47–54. https://doi.org/10.1016/S0011-9164(00)00134-X

Stillwell, A. S., & Webber, M. E. (2016). Predicting the specific energy consumption of reverse osmosis desalination. *Water*, *8*(12), 601. https://doi.org/10.3390/w8120601

Stratis, P. N., Dokou, Z. A., Karatzas, G. P., Papadopoulou, E. P., & Saridakis, Y. G. (2017). PTC simulations, stochastic optimization and safety strategies for groundwater pumping management: Case study of the Hersonissos Coastal Aquifer in Crete. *Applied Water Science*, *7*(5), 2425–2435. https://doi.org/10.1007/s13201-016-0438-8

Tomaszkiewicz, M., Abou Najm, M., & El-Fadel, M. (2014). Development of a groundwater quality index for seawater intrusion in coastal aquifers. *Environmental Modelling & Software*, *57*, 13–26. https://doi.org/10.1016/j.envsoft.2014.03.010

Triki, C., Zekri, S., Al-Maktoumi, A., & Fallahnia, M. (2017). An artificial intelligence approach for the stochastic management of coastal aquifers. *Water Resources Management*, *31*(15), 4925–4939. https://doi.org/10.1007/s11269-017-1786-3

United States Geological Survey. (2012). SEAWAT: A computer program for simulation of three-dimensional variable-density ground-water flow and transport [Software]. U.S. Geological Survey Software Release. Retrieved from https://www.usgs.gov/software/seawat-computer-program-simulation-three-dimensional-variable-density-ground-water-flow

Yang, Y., Song, J., Simmons, C. T., Ataie-Ashtiani, B., Wu, J., Wang, J., & Wu, J. (2021). A conjunctive management framework for the optimal design of pumping and injection strategies to mitigate seawater intrusion. *Journal of Environmental Management*, *282*, 111964. https://doi.org/10.1016/j.jenvman.2021.111964

Yang, Y., Wu, J., Lin, J., Wang, J., Zhou, Z., & Wu, J. (2018). An efficient simulation–optimization approach for controlling seawater intrusion. *Journal of Coastal Research*, *84*(sp1), 10–18. https://doi.org/10.2112/SI84-002.1

Yao, Y., Andrews, C., Zheng, Y., He, X., Babovic, V., & Zheng, C. (2019). Development of fresh groundwater lens in coastal reclaimed islands. *Journal of Hydrology*, *573*, 365–375. https://doi.org/10.1016/j.jhydrol.2019.03.062

Yin, J., Pham, H. V., & Tsai, F. T. C. (2020). Multiobjective spatial pumping optimization for groundwater management in a multiaquifer system. *Journal of Water Resources Planning and Management*, *146*(4), 04020013. https://doi.org/10.1061/(ASCE)WR.1943-5452.0001180

Yu, W., Baù, D., Mayer, A. S., Mancewicz, L., & Geranmehr, M. (2023). Dataset for 'Investigating the impact of seawater intrusion on the operation cost of groundwater supply in island aquifers' [Dataset]. Figshare. https://doi.org/10.6084/m9.figshare.23862975.v1

Zekri, S., Triki, C., Al-Maktoumi, A., & Bazargan-Lari, M. R. (2015). An optimization-simulation approach for groundwater abstraction under recharge uncertainty. *Water Resources Management*, *29*(10), 3681–3695. https://doi.org/10.1007/s11269-015-1023-x